

Quasifree knockout of charged particles from ${}^4\text{He}$ with 100 MeV protons

D. M. Whittal, A. A. Cowley, J. V. Pilcher, S. V. Förtsch,
F. D. Smit, and J. J. Lawrie

National Accelerator Centre, Faure, 7131 South Africa

(Received 22 March 1990)

Exclusive measurements have been made of ${}^4\text{He}(p,2p)$, (p,pd) , (p,pt) , and (p,ph) at 100 MeV. The primary protons were measured at two angles, 45° and 60° , in coincidence with secondary protons, deuterons, tritons, or helions covering a wide range of angles on the opposite side of the beam, from -15° to -90° in plane, and from 0° to 30° out of plane. The satisfactory agreement in shape between the measured energy-sharing distributions and results of distorted-wave impulse approximation calculations suggests that this formalism is adequate for modeling the quasifree knockout reactions induced by 100 MeV protons on ${}^4\text{He}$. It is found that $(70\pm 10)\%$ of the inclusive continuum yields in ${}^4\text{He}(p,p')$ is attributable to quasifree scattering, with $\sim 30\%$ arising from multiple scattering. At low energies of the scattered proton, the knockout of nucleons constitutes over 90% of the quasifree component, whereas at high energies the knockout of deuterons, tritons, and helions dominates the yield. Consequently the cluster knockout contributions fill in the yield at higher energies in the inclusive spectra, and quasifree peaks are not discernible.

I. INTRODUCTION

The mechanisms leading to the formation of continuum spectra from medium-energy proton-nucleus reactions have become of increasing interest in recent years. The continuum background underlying the giant resonances, for example, limits the accuracy to which the strengths of these states may be determined.¹ An understanding of the reaction dynamics of continuum excitations is thus vital for the proper subtraction of the background. The complexity of these continuum (or preequilibrium) excitations poses a formidable theoretical challenge, however, as they originate from neither purely direct nor purely compound-nucleus reactions.

Most approaches to the problem² have envisaged continuum emission as resulting from a sequence of particle-hole excitations, with a certain probability of emission after each step. Semiclassical formalisms include the well-known exciton³ and geometry-dependent hybrid models.⁴ More recently, quantum mechanical theories such as the statistical multistep formalism of Feshbach, Kerman, and Koonin⁵ have been developed.

It has long been recognized^{2,6,7} that most of the continuum yield is generated by the first few steps in the sequence of particle-hole excitations. In many situations, particle emission after the first collision dominates the cross section, becoming increasingly important with decreasing target mass, towards forward detection angles, and in the higher-energy regions of continuum spectra. It thus becomes crucial that model calculations should estimate the proportion of first-step emission accurately. For example, overestimation of this step has been blamed⁸ for discrepancies between semiclassical calculations and angle-integrated cross sections from recently measured (p,n) data between 80 and 160 MeV.

Further insight into the importance of the first step can be gained from studies of quasifree scattering (which, in

the context of preequilibrium models, could be called "first-step emission"). The quasifree scattering model⁹ concentrates on the physics of a single nucleon-nucleon ($N-N$) or nucleon-cluster interaction, and is expressed theoretically in the distorted-wave impulse approximation (DWIA),^{10,11} which would be expected to describe this "first step" more accurately than in the more general preequilibrium models. In this model, all subsequent steps are lumped into the so-called multiple scattering component of the cross section, which enters the DWIA in the form of the distorting optical potentials. Thus knowledge of the relative contribution of quasifree scattering and multiple scattering to proton continuum spectra may provide guidance in the tuning of the various preequilibrium models.

In the proton incident energy range between 100 and 200 MeV, however, the extent to which quasifree scattering is seen in the inclusive measurements of continuum spectra is the subject of some debate. Although the presence of a quasifree scattering component in continuum spectra is usually indicated¹² by a broad peak with a position roughly given by $N-N$ kinematics, Segel *et al.*^{13,14} have measured featureless continuum spectra for ${}^{58}\text{Ni}$ at 150 MeV, even at forward angles. On the other hand, quasifree peaks have been identified¹⁵ in spectra from the same target at lower energies (90 and 100 MeV), which should be less likely. Segel *et al.* did see quasifree peaks for the lighter targets, ${}^9\text{Be}$ and ${}^{12}\text{C}$, however, as did Förtsch *et al.*¹⁶ for ${}^{12}\text{C}(p,p')$ at both 90 and 200 MeV. Below 60 MeV, distortion effects seem to be severe enough¹⁷ to obscure the signature of quasifree scattering altogether.

In an attempt to clarify the importance of quasifree scattering around 100 MeV, Wesick *et al.*¹⁸ measured cross sections and analyzing powers from the reactions ${}^2\text{H}$, ${}^3,4\text{He}(p,p')$, and ${}^3,4\text{He}(p,d)$ for 100 and 150 MeV protons. They found quasifree peaks which tracked with $N-$

N kinematics in the yields from the ^2H and ^3He targets, but in the case of ^4He , there was no clear quasifree peak, which disagreed with their DWIA calculations. Analyzing power data were also taken, but these were not as fruitful as had been hoped in distinguishing quasifree scattering from multiple scattering contributions, because the expected multiple scattering signature of small analyzing power at low outgoing energy was also predicted by the DWIA calculations for the one-step process.

The questions left open by that experiment inspired the present coincidence measurements. Most important of these questions is the reason why no clear quasifree peaks were seen in the $^4\text{He}(p,p')$ spectra at either 100 or 150 MeV, even though they were predicted by DWIA calculations for quasifree nucleon knockout. In all cases, the high-energy portions of the measured spectra were enhanced with respect to the calculations. Some of the discrepancies were reduced by the incoherent addition of a (p,pd) contribution to the (p,pN) predictions, which filled in part of the “missing” high-energy yield and also gave a better fit to the analyzing power data. It was speculated that the inclusion of other cluster knockout reactions (p,pt) and (p,ph) might contribute further toward explaining the flat spectra from ^4He , by filling in even higher-energy portions of the inclusive cross sections. Another possible source of high-energy protons is from the unbound states^{19,20} of ^4He with excitation energy between 20 and 30 MeV.

Clearly, much of the interesting physics is inaccessible with single-detector inclusive measurements. We have thus extended these studies to exclusive particle-particle correlation measurements. The main objectives of the experiment were as follows: first, to determine whether the DWIA is valid over the angular ranges required for calculating the inclusive spectra (and if so, to extract spectroscopic factors); and secondly, to determine the relative contributions of nucleon knockout, cluster knockout, and multiple scattering to the inclusive cross sections.

The measurements which are presented here are for $^4\text{He}(p,2p)$, (p,pd) , (p,pt) , and (p,ph) at 100 MeV, for primary proton angles of 45° and 60° , secondary in-plane angles ranging from -15° to -90° , and secondary out-of-plane angles extending from 0° to 30° . Previous measurements^{21,22} of $^4\text{He}(p,2p)$ below 200 MeV have been for quasifree symmetric angles only, i.e., geometries for which zero recoil momentum is possible at equal energies of the detected protons.

In Sec. II we present details of the experiment and the replay of the data. We present the experimental results in the form of energy-sharing distributions for which the quasifree knockout locus has been projected onto the axis of the primary proton energy. Section III contains a brief description of the theory, and in Sec. IV we describe the DWIA calculations which are compared, in Sec. V, with the experimental energy-sharing distributions. In Sec. VI we then integrate over the solid angle of the secondary particle for each reaction channel, thus reconstructing the quasifree part of the inclusive (p,p') spectra. We show that quasifree scattering accounts for most of the yield. Upon adding a multiple scattering contribution, which we estimate from our data, we reproduce the in-

clusive spectra of Wesick *et al.*¹⁸ to within $\sim 10\%$. The conclusions which may be inferred from our findings, and a summary of the work, are presented in Sec. VII.

II. EXPERIMENTAL PROCEDURE

A beam of 100 MeV protons with a typical intensity of ~ 60 nA was delivered by the separated-sector cyclotron (SSC) of the National Accelerator Centre.²³ The layout of the facility has been described elsewhere.²⁴ The energy of the extracted beam was calculated from the length of the extracted orbit and the period of the beam in the SSC. An uncertainty of 0.4 MeV arises from uncertainties in the centering of the beam and in the beam phase relative to the rf phase. The energy spread in the extracted beam was estimated to be ~ 100 keV and was reduced somewhat by emittance-limiting slits in the beamline which leads to the 1.5-m scattering chamber. The spot size on target was generally smaller than 4 mm wide by 2 mm high and the divergence of the beam was $\sim 0.2^\circ$ horizontally and $\sim 0.3^\circ$ vertically. The position of the spot was never more than 0.5 mm off-center and we estimate a directional stability of $\leq 0.1^\circ$. The beam was stopped at a distance of 6.34 m from the target by sections of aluminum with a total thickness of 22.8 cm and a diameter of 18.4 cm.

An aluminum gas cell with entrance and exit windows of 25- μm Havar contained the target of high-purity (99.995%) helium gas. An absolute pressure transmitter enabled the pressure to be monitored continuously to $< 0.25\%$. The gas in the cell was assumed to be in thermal equilibrium with its environment.

For particle identification over a wide dynamic range for protons, deuterons, tritons, and helions, we used triple-element detector telescopes consisting of two silicon surface barrier detectors, both of area 300 mm², followed by a 51-mm diam by 127-mm long NaI(Tl) crystal. The front silicon detectors were 100 μm thick, and the second detectors were either 500 or 1000 μm thick. The NaI detectors were integral line assemblies with thin (6- μm) Havar entrance windows and μ -metal shielding.

We employed two primary detector telescopes, 30° apart, one of which was equipped with active collimation (6-mm thick scintillator), and four secondary telescopes in the configuration illustrated in Fig. 1: two in-plane telescopes, 15° apart, and two out-of-plane telescopes placed 15° and 30° directly above the forward in-plane detector telescope. Double-aperture brass collimators defined an appropriate length of the line target and the effective angular resolution²⁵ in this coincidence experiment was always $\leq 3^\circ$. The width of the front aperture (which consists of vertical slits) is the principal factor in determining the target length parameters. As it was impossible to satisfy all the desired requirements for the collimators at all geometries with a single set of front slits, two sets were required. Coincidence target lengths were always in the range 6–11 mm. The collimators subtended 1.5 msr at the target, with a distance of 25 cm between the front vertical slits and the circular rear apertures of diameter 14 mm. The front slits varied in width from 5 to 24 mm.

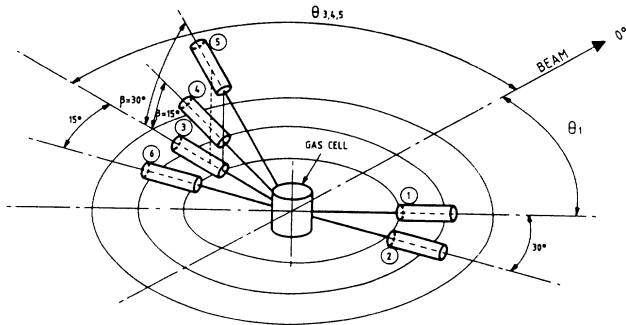


FIG. 1. The configuration of the detector telescopes. Primary telescopes 1 and 2 are coplanar with both the beam and secondary telescopes 3 and 6. Secondary telescopes 4 and 5, mounted directly above telescope 3, are out of plane by 15° and 30° , respectively.

Standard fast coincidence electronics were used to process the timing and linear energy signals from the detectors. Tail pulse generators fed pulses into the preamplifiers of the six thicker silicon detectors and the six NaI detectors for the purpose of correcting for pileup and electronic dead time during replay. The pulsers were triggered at a rate proportional to the beam current. An online computer wrote event-by-event data to tape.

Protons scattered from a polythene target provided the means for energy calibration of the NaI detectors; peaks from elastic scattering off hydrogen, helium, and carbon, and inelastic scattering to several of the excited states of carbon were used. Although the response function of NaI for protons in the energy range up to 100 MeV is slightly nonlinear, linear fits were found to be adequate for the purposes of this experiment (all the points, including those not used in the fitting routine, generally lay within 2% of the lines). The response of the NaI detectors to deuterons and helions was determined from the reactions ${}^4\text{He}(p,d)$, ${}^{12}\text{C}(p,d){}^{11}\text{C}^*(\text{g.s. and } 2.00 \text{ MeV})$, and ${}^{12}\text{C}(p,h)$ at various angles for the detected particles. The response to deuterons is consistently $\sim 4\%$ greater, and that of helions $\sim 20\%$ less than two protons of the same energy, which is in agreement with results^{26,27} for CsI(Tl). As we had no peaks upon which to base a direct calibration for the response to tritons, we assumed it to have the same trend as for deuterons, with twice the difference in slope as between the proton and deuteron responses, which is roughly the trend²⁷ found in CsI (i.e., the triton response was assumed to be $\sim 8\%$ greater than that for protons). Although this procedure might seem rather arbitrary, it should be noted that the energy-sharing spectra (Sec. V) were obtained from projections onto the energy axis of the primary proton; calibrations for the other particles merely needed to be good enough to ensure reasonably straight knockout loci in the summed-energy spectra (see below).

During replay of the tapes, the peaks due to elastically scattered protons from the ${}^4\text{He}$ target and also, when they were discernible, the peaks from the $(p,d)(\text{g.s.})$ reaction were continuously monitored. These peaks were visible because of random coincidences, and were used to

adjust the calibration parameters of the NaI detectors for gain drifts in the photomultiplier tubes.

After initial replay of all the data, we chose a representative subset of the 408 two-dimensional energy-sharing spectra for further analysis, which enabled us to follow the trends in the data. The selection of proton-proton spectra is shown in Fig. 2. The reason for neglecting the most forward-angle spectra was the poor statistical accuracy of those data. At the secondary angles $(\theta_S; \beta_S) = (-35^\circ; 0^\circ)$, there were two entirely independent sets of data involving different telescopes and slit widths, which was a useful indication of the systematic error (see below).

The two-dimensional (2D) energy-sharing spectra were converted into spectra of summed-energy versus primary proton energy, where

$$E_{\text{Sum}} = E_P + E_S + E_R - Q, \quad (1)$$

and the subscripts P , S , and R refer to the primary, secondary, and recoil particles, respectively. E_R was calculated with the use of relativistic kinematics. A typical 2D energy-sharing spectrum and the corresponding summed-energy spectrum are shown in Fig. 3. Deviations from the straight line at 100 MeV reflect calibration errors and nonlinearities. For projecting the knockout

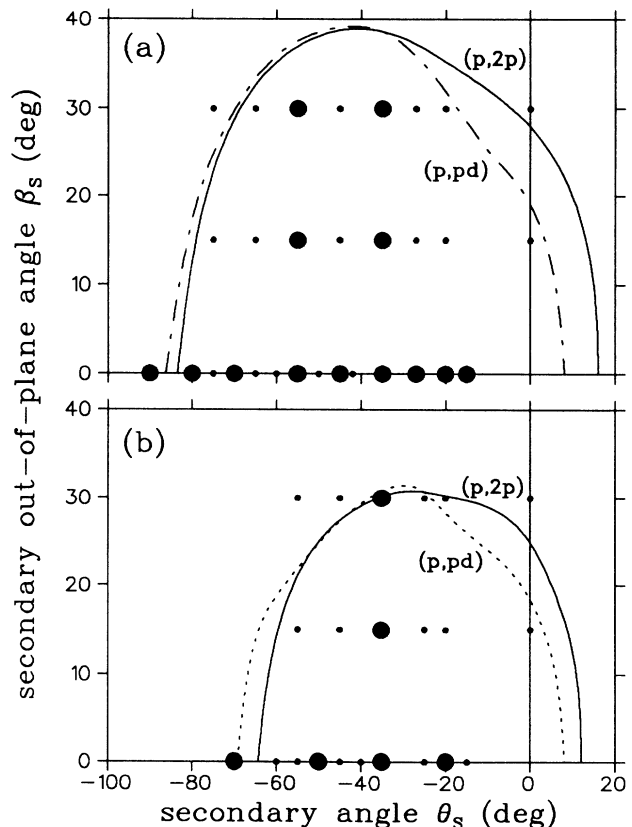


FIG. 2. Selection of a subset of the data. The available geometries for (a) $\theta_P = 45^\circ$ and (b) $\theta_P = 60^\circ$ are indicated by the dots, with the selected spectra shown as large dots. The loci within which recoils of $< 200 \text{ MeV}/c$ are possible are indicated for the $(p,2p)$ and (p,pd) reactions.

locus onto the primary proton energy axis, each summed-energy range was subjectively chosen to include the full width of the locus, as shown by the horizontal dashed lines.

The vertical dashed lines indicate the ranges of primary proton energies which were included in the projections. Electronic thresholds in the primary and secondary telescopes determine the extremes of the energy range. At ~ 14 MeV, there is a gap in the data between the “low-energy” and “high-energy” portions of the primary proton spectrum, caused by electronic thresholds for the NaI detectors. This gap was typically 2–4 MeV wide, including the broadening due to binning effects (the energy bins are 1 MeV wide).

Correction for accidental coincidences in the prompt timing peak was performed by subtracting events from neighboring beam bursts of the cyclotron rf structure. To correct for reaction losses in the NaI crystals, we used the empirical formula of Green *et al.*,²⁸ which gives values for the reaction tail within 2% of Cameron *et al.*²⁹ at 89 and 104 MeV, and a value within 2% of that quoted in the Janni tables³⁰ for 100 MeV protons in NaI. The corrections required for the secondary deuterons, tritons, and helions were assumed to be the same as for protons of the same energy. This is a similar approach to that of Segel *et al.*,¹³ except that they ignored altogether the

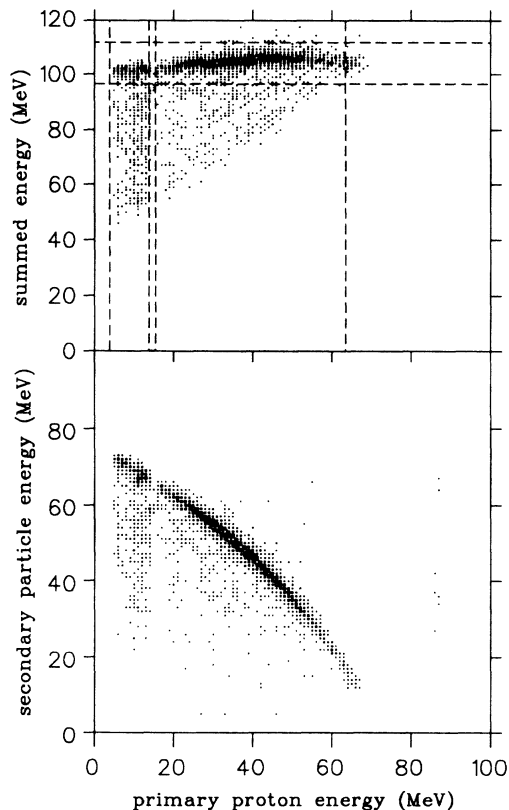


FIG. 3. A typical 2D energy-sharing spectrum (below) and summed-energy spectrum (above). The quasifree knockout locus is clearly visible. The dashed lines indicate the regions of the locus that were chosen for projection onto the energy axis of the primary proton, as described in the text.

TABLE I. Summary of the systematic errors.

Source of error	% error
Finite resolution effects	3
Slit penetration	$\ll 1$
Reaction tail correction	$\ll 1$
Particle identification gates	3
Energy scale	4
Solid angles	2
Effective target length	3
Pressure	2
Temperature	0.3
Integrated charge	~ 0.2
Dead time corrections	4
Subtraction of accidentals	2
Linear sum	24
Total systematic error	8

tails due to helions, which is justifiable on the grounds of the shorter ranges for $Z=2$ particles. The spectra were also corrected for energy losses in the 25- μm Havar foil of the gas cell window. For the lowest primary proton energies in the energy-sharing spectra (5 MeV) the correction was ~ 1 MeV, becoming negligible for proton energies above 20 MeV.

Systematic errors are summarized in Table I. If we assume that they are uncorrelated, they add in quadrature to give an overall systematic error of 8%. There are obviously some correlations, however, particularly among the uncertainties in the energy scale, the solid angles, and the effective target length, which have common components in misalignments of the beam and collimators. Adding these three uncertainties linearly and then summing in quadratures raises the total figure to 11%. Consequently, the total systematic error is conservatively estimated to be $< 10\%$.

III. THEORY

We have used the computer program³¹ THREEDD to perform DWIA calculations. As the theoretical basis of this program is well documented,^{32–34} we give only a brief description here.

We denote the reaction by $A(a,cd)B$ where $A = B + b$. The differential cross section is given by

$$\sigma_{BA} = \frac{2\pi}{\hbar v} |T_{BA}|^2 \omega_B, \quad (2)$$

where v is the relative velocity of a and A in the entrance channel, T_{BA} is the reduced transition amplitude, and ω_B is the phase space factor.

Applying the factorization approximation, which requires³² the effect of the distorting potentials on the two-body interaction to be negligible, we may write (for an unpolarized beam)

$$|T_{BA}|^2 = C^2 S \sum_{\rho_a \rho_c \rho_d' JM} \frac{1}{(2J+1)(2S_a+1)} \left| \sum_{\sigma_a \sigma_c \sigma_d' \Lambda \sigma_b} (2\Lambda+1)(L \Lambda S_b \sigma_b | JM) T_{\sigma_a \sigma_c \sigma_d' \rho_a \rho_c \rho_d'}^{L \Lambda} \langle \sigma_c \sigma_d' | t | \sigma_a \sigma_b \rangle \right|^2, \quad (3)$$

where $C^2 S$ is the spectroscopic factor for the final state in B , L is the relative angular momentum (projection Λ) of b and B , J is the angular momentum (projection M) of the target, S_i are the spins, with projections ρ_i and σ_i for particles i (as defined by Chant and Roos³⁴), t is the two-body operator for the free N - N scattering process (by the impulse approximation), and the primes indicate quantities which are expressed with respect to different sets of axes, as follows: The unprimed \hat{z} axis is along the beam direction, whereas the \hat{z}' and \hat{z}'' axes are in the directions of propagation of particles c and d , respectively.

The quantity $T^{L\Lambda}$ is defined by

$$T_{\sigma_a \sigma_c \sigma_d' \rho_a \rho_c \rho_d'}^{L \Lambda} = (2L+1)^{-1/2} \int \chi_{\sigma_c \rho_c}^{(-)*}(\mathbf{r}') \chi_{\sigma_d' \rho_d'}^{(-)*}(\mathbf{r}'') \phi_{L\Lambda}(\mathbf{r}) \chi_{\sigma_a \rho_a}^{(+)}(\gamma \mathbf{r}) d\mathbf{r}, \quad (4)$$

where the χ_{ij} are distorted waves, ϕ is the spatial part of the bound-state wave function of particle b , and $\gamma = B/A$. THREEDDEE performs a direct Gaussian integration of Eq. (4). The final result for the triple differential cross section is thus

$$\frac{d^3 \sigma}{d\Omega_c d\Omega_d dE_c} = C^2 S K \sum_{\rho_a \rho_c \rho_d' JM} \left| \sum_{\sigma_a \sigma_c \sigma_d' \sigma_b \Lambda} (L \Lambda S_b \sigma_b | JM) D_{\sigma_c \sigma_c'}^{(1/2)*}(R_{ac}) D_{\sigma_d \sigma_d'}^{(1/2)*}(R_{ad}) T_{\sigma_a \sigma_c \sigma_d' \rho_a \rho_c \rho_d'}^{L \Lambda} \right. \\ \left. \times \langle \sigma_c \sigma_d' | t | \sigma_a \sigma_b \rangle \right|^2, \quad (5)$$

where K is a kinematic factor (also containing constant terms which drop out of the summations for a specific final state in B), the D_{mn} are rotation matrices, and the R_{aj} are rotations of the sets of axes which were defined for particle j into the set of axes for particle a .

The half-off-shell two-body t matrix is approximated by interpolation of on-shell nucleon-nucleon phase shifts, with a choice of two prescriptions^{35,36} for the center-of-mass energy: In the final-energy prescription (FEP), $E_{c.m.}$ is taken as the relative c.m. energy of the emitted particles c and d ; in the initial-energy prescription (IEP), $E_{c.m.}$ is the relative c.m. energy of the incident particle a and the struck particle b , where the fact that b is off the mass shell is ignored, and the scattering angle is taken to be the same as in the FEP.

If spin-orbit interactions are ignored, the expression may be simplified, as it is no longer necessary to sum the elements of the two-body t matrix coherently with the distorted-wave integral; this leads to the appearance of the two-body cross section as a multiplicative factor:³²

$$\frac{d^3 \sigma}{d\Omega_c d\Omega_d dE_c} = C^2 S K' \frac{d\sigma}{d\Omega_{1-2}} \sum_{\Lambda} |T_{BA}^{\alpha L \Lambda}|^2, \quad (6)$$

where K' is a different kinematic factor from K . The factor $|T_{BA}^{\alpha L \Lambda}|^2$ is the distorted momentum distribution, where α represents additional quantum numbers. The particles 1 and 2 in the two-body cross section are a and b for the IEP or c and d for the FEP approximation.

Finally, to obtain inclusive cross sections, the triple differential cross sections (5) and (6) may be integrated over the solid angle of the unobserved particle:

$$\frac{d^2 \sigma}{d\Omega_c dE_c} = \int \frac{d_3 \sigma}{d\Omega_c d\Omega_d dE_c} d\Omega_d, \quad (7)$$

where, as discussed in Sec. VI A, the distortion of the unobserved particle needs to be modified appropriately.

IV. CALCULATIONS

Two types of DWIA calculations are discussed in this paper: first, in this section, calculations of the triple differential cross sections for comparison with the coincidence energy-sharing distributions generated from the present data (for the quasifree knockout of protons, deuterons, tritons, and helions); and secondly, in Sec. VI, calculations based on these comparisons, of the inclusive (p, p') cross sections for comparison with the inclusive spectra from Wesick *et al.*¹⁸

In the program THREEDDEE,³¹ distorted-wave functions $\chi_{ij}^{(\pm)}$ [see Eq. (4)] are generated³⁴ from spin-dependent optical potentials. For the entrance channel, $p + {}^4\text{He}$ at a laboratory energy of 100 MeV, we used the optical potential given in Ref. 37, with a nonlocality³⁸ range of 0.85 fm. Furthermore, because the interaction with the knocked-out particle is explicitly included in the two-body t matrix, we adjusted the well depths^{10,39} by the ratio m_B/m_A .

For the exit channels of the ($p, 2p$) reaction, energy-dependent optical potentials were derived⁴⁰ from Refs. 37 and 41, and these are given in Table II. Also listed in Table II are the energy-dependent potentials^{40,42} for the $p + d$ final state in the (p, pd) reaction. For the $d + d$ scattering, a folding model potential⁴³ was used, with a nonlocality range of 0.54 fm. For the (p, pt) and (p, ph) reactions, we used plane waves for the $p + p$ and $p + n$ exit channels; for the $t + p$ and $h + n$ legs of the final states, we used the same potentials as for $p + t$ (Table II), with the energy scaled appropriately.

The bound-state wave function $\phi_{L\Lambda}(\mathbf{r})$ for ${}^4\text{He}(p, 2p)$ is theoretically the overlap integral of the ${}^4\text{He}$ and nnp -cluster wave functions, which may be derived phenomenologically⁴⁴ from electron scattering data by fitting the ${}^4\text{He}$ charge form factor. We chose the parametrization used by van Oers *et al.*³⁷ As it is estimated⁴⁵ that the

TABLE II. Energy-dependent optical potentials used in the calculations.

$$V_{\text{opt}}(r) = -Vf(r, r_R, a_R) - i \left[W - 4W_D a_I \frac{d}{dr} \right] f(r, r_I, a_I) - (-1)^l V_{\text{ex}} f(r, r_{\text{ex}}, a_{\text{ex}}) + \left[\frac{\hbar}{m_\pi c} \right]^2 l \cdot \sigma \frac{1}{r} (V_{\text{SO}} + iW_{\text{SO}}) \frac{df(r, r_{\text{SO}}, a_{\text{SO}})}{dr} + V_C,$$

where the Woods-Saxon form factor

$$f(r, r_i, a_i) = \left[1 + \exp \left(\frac{r - r_i A^{1/3}}{a_i} \right) \right]^{-1},$$

and V_C is the Coulomb potential between a point scattered particle and a uniformly charged sphere of radius $r_C A^{1/3}$.

$p + t, h$ ($E < 65$ MeV)		
$V = 53.75 - 0.869E + 0.004E^2$	$r_R = 1.488$	$a_R = 0.144$
$W = 0.06146E^{1.365}, W_D = 0$	$r_I = 1.501$	$a_I = 0.378$
$V_{\text{ex}} = -0.065V$	$r_{\text{ex}} = 1.488$	$a_{\text{ex}} = 0.144$
$V_{\text{SO}} = 0.07566E^{1.305}, W_{\text{SO}} = 0, \beta_{\text{nonloc}} = 0.85$	$r_{\text{SO}} = 1.049$	$a_{\text{SO}} = 0.289$
	$r_C = 1.3$	
$p + t, h$ ($E \geq 65$ MeV)		
$V = 67.01 - 11.91 \ln(E)$	$r_R = 1.481$	$a_R = 0.199$
$W = 12.65 - 0.02478E + 3.413 \times 10^{-5}E^2, W_D = 0$	$r_I = 1.828$	$a_I = 0.233$
$V_{\text{ex}} = -1129E^{-1.361}$	$R_{\text{ex}} = 0.930$	$a_{\text{ex}} = 0.562$
$V_{\text{SO}} = 17.47 - 2.343 \ln(E), W_{\text{SO}} = -0.76, \beta_{\text{nonloc}} = 0.85$	$r_{\text{SO}} = 1.007$	$a_{\text{SO}} = 0.255$
	$r_C = 1.3$	
$p + d$		
$V = 1.4 + 114/\sqrt{E}$ for $E \leq 50$ MeV: $= 412.8/E^{0.75} - 5.37$ for $E > 50$ MeV.	$r_R = 1.6$	$a_R = 0.5$
$W = 0.1769E^{0.767}, W_D = 0, V_{\text{ex}} = 0$	$r_I = 1.6$	$a_I = 0.5$
$V_{\text{SO}} = 6.0, W_{\text{SO}} = 0, \beta_{\text{nonloc}} = 0.85$	$r_{\text{SO}} = 1.6$	$a_{\text{SO}} = 0.5$
	$r_C = 1.72$	

nnp cluster in ${}^4\text{He}$ is in the triton state $\sim 80\%$ of the time ($> 90\%$ for low-momentum components), we have also used this bound-state wave function to describe the triton in ${}^4\text{He}$, for the (p, pt) calculations. Furthermore, because its derivation⁴⁶ assumes isospin invariance, it has also been used as the overlap integral for calculating the (p, pn) and (p, ph) cross sections.

For the $d + d$ bound-state wave function in the (p, pd) calculations, we Fourier transformed the momentum distribution measured for ${}^4\text{He}(p, pd)$ at 156 MeV by Frascaria *et al.*,²² which is a Gaussian with FWHM = 210 MeV/c, to get

$$U(r)/r = 0.767 \exp(-0.204r^2). \quad (8)$$

The two-body t matrix for the knockout of a nucleon was calculated from experimental $N-N$ phase shifts. For cluster knockout, values were interpolated from experimental cross sections for the elastic scattering of $p + d$ (Ref. 47), $p + t$ (Refs. 48 and 49), and $p + h$ (Refs. 49 and 50).

V. COINCIDENCE DATA: RESULTS AND DISCUSSION

A. ${}^4\text{He}(p, 2p)^3\text{H}$

A representative selection of the energy-sharing distributions for the primary angle $\theta_p = 45^\circ$ is shown in Fig. 4.

Cross sections are given in the laboratory system. The data exhibit a broad bump which is characteristic of quasifree knockout from an s state, as expected. As $|\theta_S|$ increases, the kinematic dependence is clearly seen: The position of the peak moves from primary proton energy $T_p \sim 30$ MeV up to ~ 55 MeV at $\theta_S = -70^\circ$ and it disappears above the high-energy cutoff for $|\theta_S| \geq 80^\circ$. The peak cross section continues to rise beyond the quasifree angle ($45^\circ; -27^\circ; 0^\circ$) to a maximum of $\sim 160 \mu\text{b sr}^{-2} \text{MeV}^{-1}$ for $|\theta_S| \sim 35^\circ$ to 45° , and then falls rapidly with increasing angle. The falloff with out-of-plane angle β_S is also quite sharp, and the quasifree bump becomes less pronounced, as can be seen at $\theta_S = -35^\circ$ and -55° . Clearly, most of the yield is indeed concentrated in the region corresponding to recoil momenta < 200 MeV/c (see Fig. 2), as expected. At T_p below the energy gap (< 12 MeV), the fluctuating cross section may be associated with sequential decay from ${}^4\text{He}(p, p'){}^4\text{He}^*$; several states¹⁹ in the excitation region of 20–22 MeV have been observed,²⁰ and would yield low-energy protons in this region of T_p . For $\beta_S = 30^\circ$ the effect of an electronic cutoff in one of the particle identification spectra progressively worsens towards lower primary proton energies (< 42 MeV) and these data points should be treated with circumspection.

The energy-sharing distributions for primary angle $\theta_p = 60^\circ$ are shown in Fig. 5. There is no quasifree angle in this case, but the recoil momentum reaches a minimum of 23 MeV/c at $\theta_S = -12^\circ$. Thus the minimum recoil momentum at each angle increases with $|\theta_S|$ for the entire set of data presented. The characteristic quasifree bump is not as clear in this set of data, and the peak yield is lower than at $\theta_p = 45^\circ$, reaching $\sim 100 \mu\text{b sr}^{-2}\text{MeV}^{-1}$ at $(60^\circ; -35^\circ; 0^\circ)$. The falloff towards out-of-plane angles is as rapid as for $\theta_p = 45^\circ$, and towards increasing $|\theta_S|$ it is even more rapid than for $\theta_p = 45^\circ$, which is consistent again with the interpretation of Fig. 2.

In Figs. 4 and 5 the DWIA calculations with the final-energy prescription for the two-body scattering are plotted as the solid curves, and those for the initial-energy prescription are plotted as dashed curves. There is very little difference in shape between the curves for each prescription; both give satisfactory overall agreement with the data over the whole angular range covered. The calculated distributions are in some cases narrower than the experimental distributions and they peak at a lower energy T_p . They also tend to turn upwards at either end of the energy scale, particularly at forward angles, a trend which is not generally reflected in the data. This discrepancy (see Sec. VF) is caused mainly by the

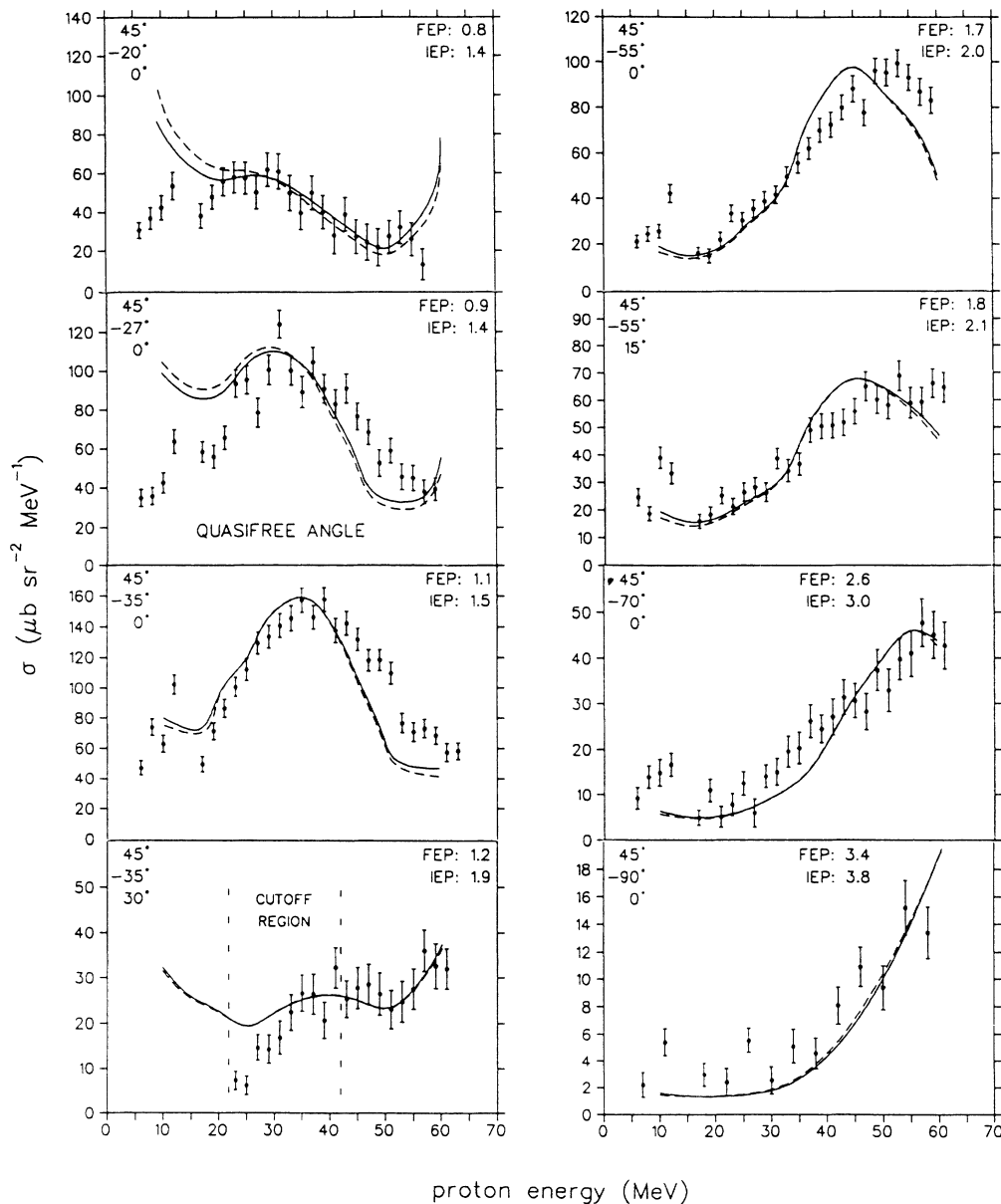


FIG. 4. Experimental cross sections for the quasifree knockout reaction ${}^4\text{He}(p, 2p){}^3\text{H}$ at primary angle $\theta_p = 45^\circ$ are shown as points with statistical error bars. The angles given in each plot are (from top to bottom) primary proton angle θ_p , secondary in-plane angle θ_S , and secondary out-of-plane angle β_S . DWIA calculations with the final-energy prescription (FEP, solid curves) and the initial-energy prescription (IEP, dashed curves) are normalized to the data with the indicated spectroscopic factors.

energy-dependent optical potential of the low-energy particle in the final state.

The spectroscopic factors for the two prescriptions (indicated on the plots) are almost the same at large angles, but differ by nearly a factor of 2 at the smallest angles, which is as expected: Off-shell effects on the two-body interaction are emphasized³⁶ at forward angles, and are particularly significant when the binding energy is relatively high, as is the case for ${}^4\text{He}$. The two on-shell prescriptions are believed to represent the extremes, with the proper⁵¹ half-shell cross sections lying somewhere in between.^{36,52}

In Fig. 6 the spectroscopic factors are plotted as a function of secondary angle θ_S for each primary angle θ_P . They are angle dependent, rising more or less linearly with increasing secondary angle. The error bars represent one-third of the estimated maximum possible error in normalizing the DWIA distributions to the data. The lines are least-squares fits (weighted by the inverse relative errors) for a constant spectroscopic factor, and for a linear angle dependence, respectively. We shall return to the subject of these angle-dependent spectroscopic factors in Sec. VI.

B. ${}^4\text{He}(p, pd){}^3\text{H}$

Energy-sharing distributions are shown in Figs. 7 and 8. The general trends are similar to those for $(p, 2p)$, except that the yield tends to peak towards higher primary proton energies. The quasifree angles are $(45^\circ; -44^\circ; 0^\circ)$ and $(60^\circ; -36^\circ; 0^\circ)$; in both cases the yield reaches a maximum at those angles. The most striking feature of these data is that the cross sections at the higher primary proton energies are often comparable with the $(p, 2p)$ cross sections. The (p, pd) contribution is thus an important component of the total (p, p') yield at the higher p' energies, as postulated by Wesick *et al.*¹⁸ Although the agreement in shape between the (p, pd) data and the DWIA calculations is not as good as for proton knockout, it is still reasonable. The two-body cross section is not determined as accurately as in $(p, 2p)$, which probably explains most of the differences between the two prescriptions.

The spectroscopic factors are not as systematic as for $(p, 2p)$, with the ratio between the two prescriptions varying between 7 and 2. As can be seen in Fig. 9, at $\theta_P = 45^\circ$ the FEP spectroscopic factors are reasonably constant,

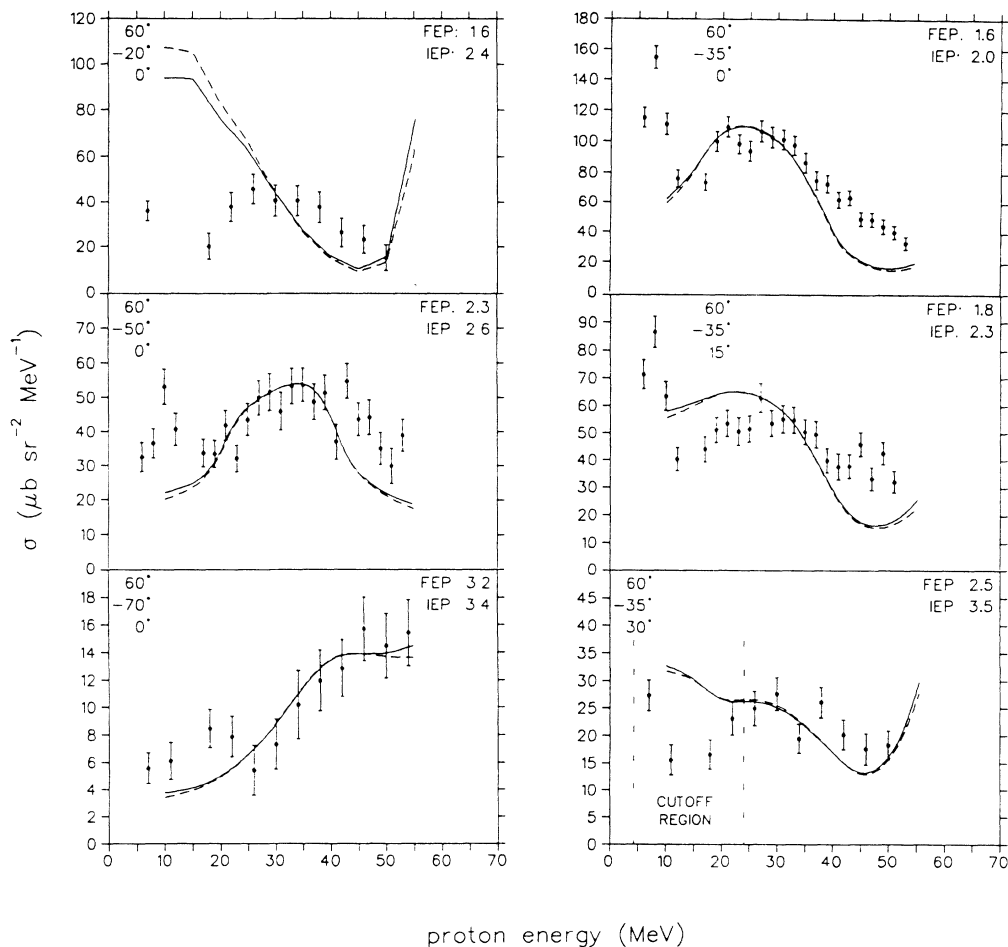


FIG. 5. Experimental cross sections and DWIA calculations for the quasifree knockout reaction ${}^4\text{He}(p, 2p){}^3\text{H}$ at primary angle $\theta_P = 60^\circ$. See caption to Fig. 4.

mostly lying within a standard deviation of 0.3; at $\theta_p=60^\circ$, they are generally higher, being clustered around 0.6. On the other hand, for the IEP at 45° , they decrease with increasing secondary angle, and at 60° there is no clear trend. The spectroscopic factor for $(60^\circ; -35^\circ; 30^\circ)$ is noticeably higher than the others, because the DWIA predicts a more rapid drop in the distorted momentum distribution than is seen in the data as it goes out of plane from the quasifree angle $(60^\circ; -35^\circ; 0^\circ)$.

C. ${}^4\text{He}(p,pt)H$

Energy-sharing distributions for the knockout of triton clusters are shown in Figs. 10 and 11. As for (p,pd) , the yield is greatest at high energies T_p and is at places comparable with $(p,2p)$; furthermore, it does not fall off as rapidly as (p,pd) towards large angles $|\theta_S|$. As for (p,pd) , the yields peak at $(45^\circ; -45^\circ; 0^\circ)$ and $(60^\circ; -35^\circ; 0^\circ)$, but at higher energies. The quasifree angles for triton knockout are a little further out, at $(45^\circ; -51^\circ; 0^\circ)$ and $(60^\circ; -44^\circ; 0^\circ)$. At large angles $(45^\circ; -70^\circ; 0^\circ)$ and $(60^\circ; -70^\circ; 0^\circ)$ the central regions of the distributions are enhanced by final state interactions between the primary and recoil protons (see Sec. V E).

For the DWIA calculations at forward angles, neither prescription describes the shape of the data very well. From $\theta_S = -35^\circ$ outwards, the agreement is reasonable, with the FEP generally being better than the IEP for primary angle 45° , and the IEP being better at 60° . The steep rise in the DWIA cross section towards high proton energy is not as pronounced in the data. This is caused by the distorted-wave integral increasing more rapidly

than would be expected from an inspection of the recoil momenta. Possibly, it indicates that the triton optical potential is no longer appropriate at such low triton energies.

The spectroscopic factors are shown in Fig. 12. They are erratic, mainly because it is difficult to normalize a curve which is rising steeply at the point where the data reach their high-energy cutoff. The normalization thus depends critically on the cutoff energy. This can be seen most clearly for $(60^\circ; -35^\circ; 30^\circ)$ and $(60^\circ; -70^\circ; 0^\circ)$, where the lower cutoffs in the data (Fig. 11) cause the extracted spectroscopic factors to be far out of line with the others. These two values were thus not used in the least-squares calculations of the average spectroscopic factors.

D. ${}^4\text{He}(p,ph)n$

The few distributions that could be extracted from the helion-knockout data are presented in Fig. 13. Generally they seem similar to the (p,pt) distributions, which is to be expected, as the physics and kinematics involved are much alike.

There is good agreement in shape between the DWIA calculations and the experimental data at $(45^\circ; -55^\circ; 15^\circ)$, and at $(45^\circ; -65^\circ; 0^\circ)$ (after final state interactions have been accounted for, as described below). At $(60^\circ; -55^\circ; 15^\circ)$ the agreement would probably also be improved if the component due to final state interactions were included.

For $\theta_p=45^\circ$, the average spectroscopic factors for the three distributions are 0.52 and 0.21 for the IEP and FEP, respectively, but these are not the values which we have used for integrating the inclusive yields (Sec. VI).

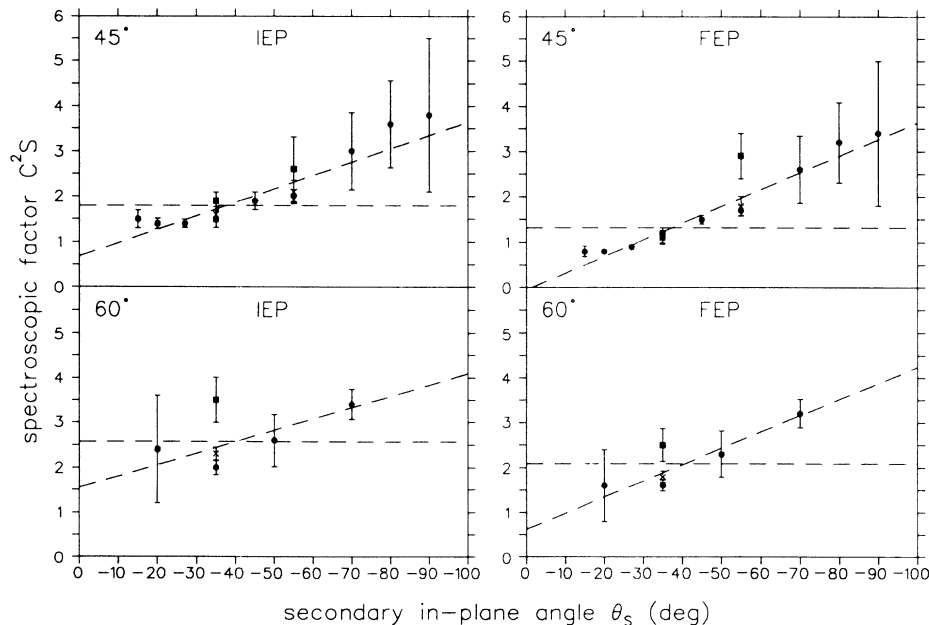


FIG. 6. Spectroscopic factors for $(p,2p)$ at primary angles 45° and 60° , for each of the two prescriptions (as indicated). The factors for in-plane angles are plotted as dots, and those for out-of-plane angles are represented by crosses (for $\beta_S = 15^\circ$), and by squares (for $\beta_S = 30^\circ$). The dashed lines are least-squares fits as described in the text.

Rather, we took the values for (p,pt) , because they are based on a wider range of distributions, and scaled them according to the difference between (p,ph) and (p,pt) at the angles for which we had both distributions. For $\theta_p = 60^\circ$, there is no (p,pt) distribution corresponding to the single (p,ph) distribution, so we used the spectroscopic factors as extracted from the (p,ph) comparisons.

E. Final state interactions

In a number of the energy-sharing distributions for three-nucleon-cluster knockout, there is evidence of some extra structure which is not caused by the quasifree

mechanism. This is particularly evident for (p,pt) at $(45^\circ; -70^\circ; 0^\circ)$, Fig. 10, and for (p,ph) at $(45^\circ; -65^\circ; 0^\circ)$, Fig. 13.

The final relative energy between the recoil nucleon and the primary proton reaches a minimum in the region of these structures. Consequently we have evaluated the final state interactions with a Watson-Migdal formalism⁵³ for the (p,ph) case to investigate whether this reaction mechanism is consistent with the observed structure. The singlet np effective range and scattering length were taken from an analysis of Lomon and Wilson.⁵⁴ The triplet contribution to the np scattering was ignored, as the singlet state is known⁵⁵ to be predominant. In Fig. 13 the contribution of these final state interactions is shown at

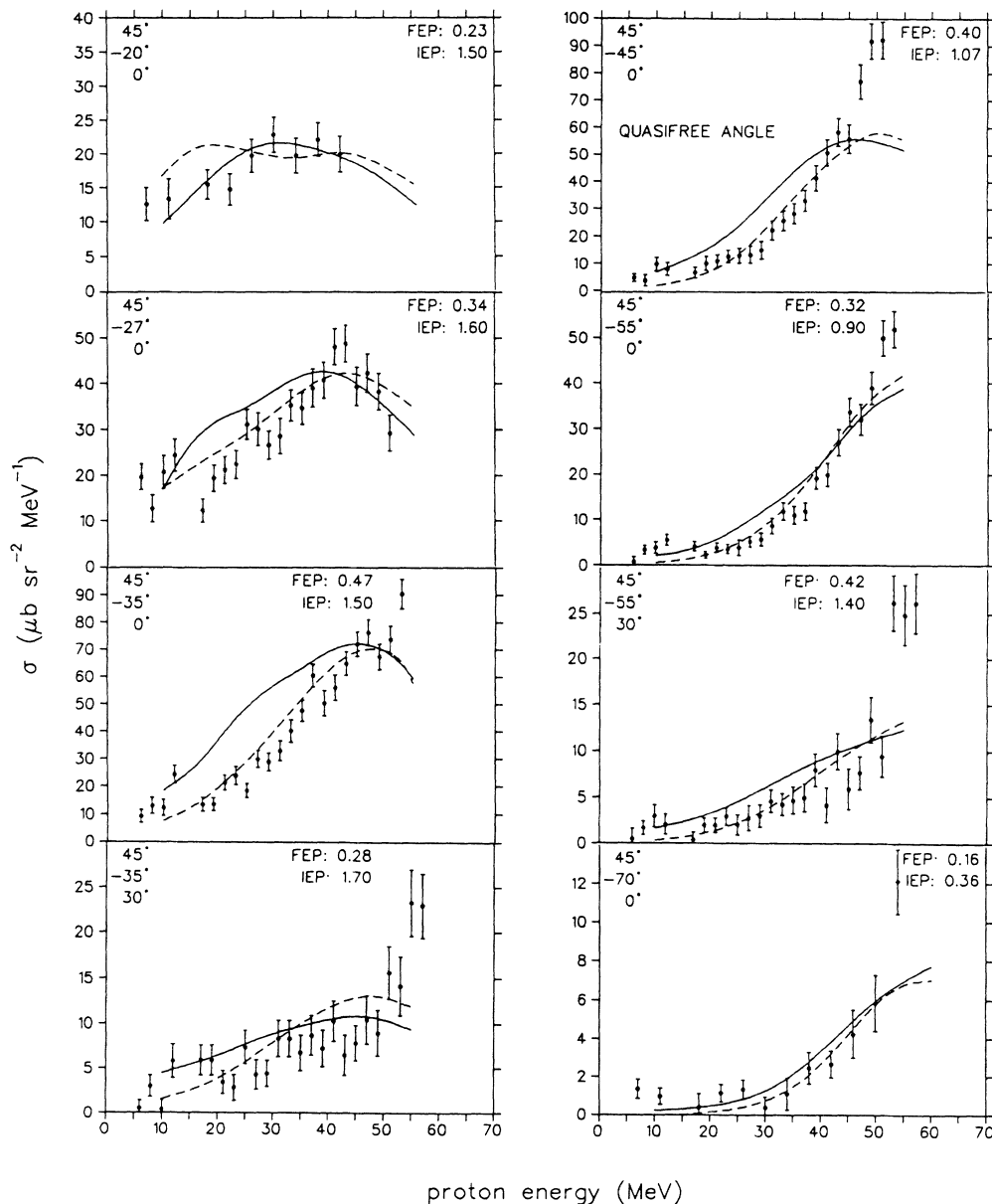


FIG. 7. Experimental cross sections and DWIA calculations for the quasifree knockout reaction ${}^4\text{He}(p,pd){}^2\text{H}$ at primary angle $\theta_p = 45^\circ$. See caption to Fig. 4.

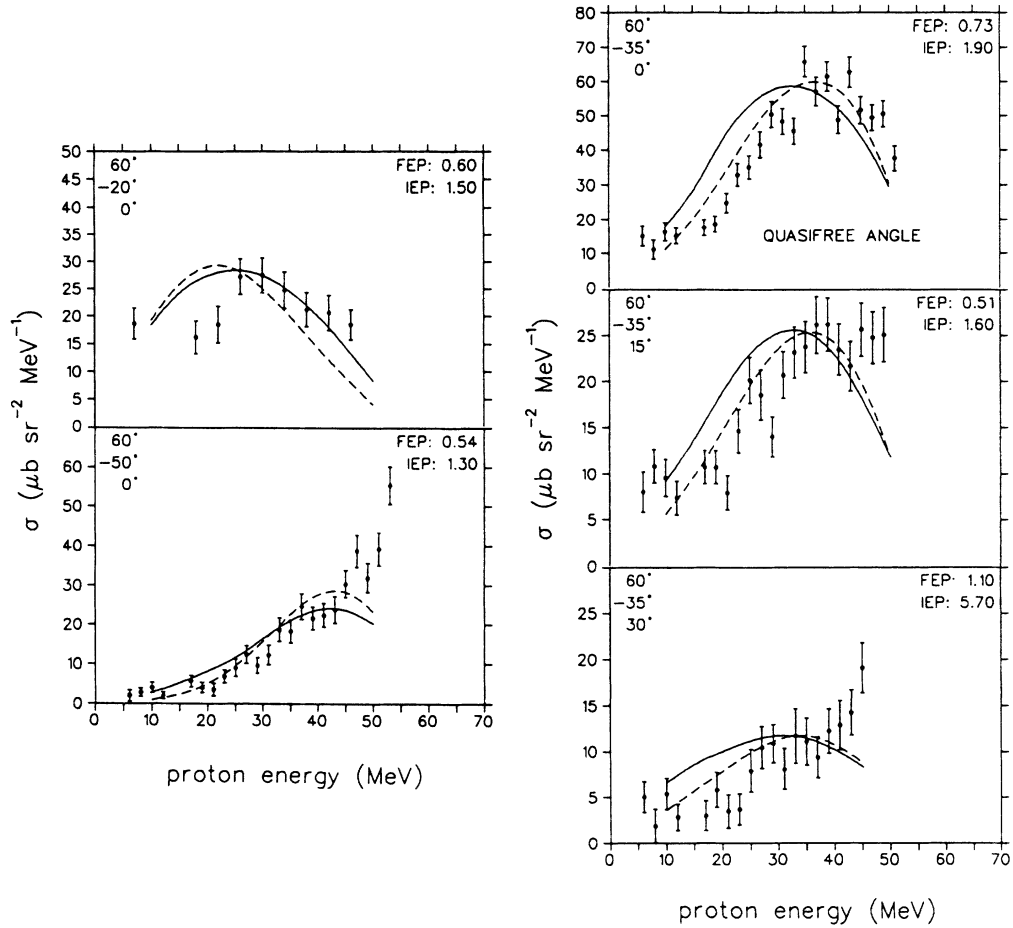


FIG. 8. Experimental cross sections and DWIA calculations for the quasifree knockout reaction ${}^4\text{He}(p,pd){}^2\text{H}$ at primary angle $\theta_p = 60^\circ$. See caption to Fig. 4.

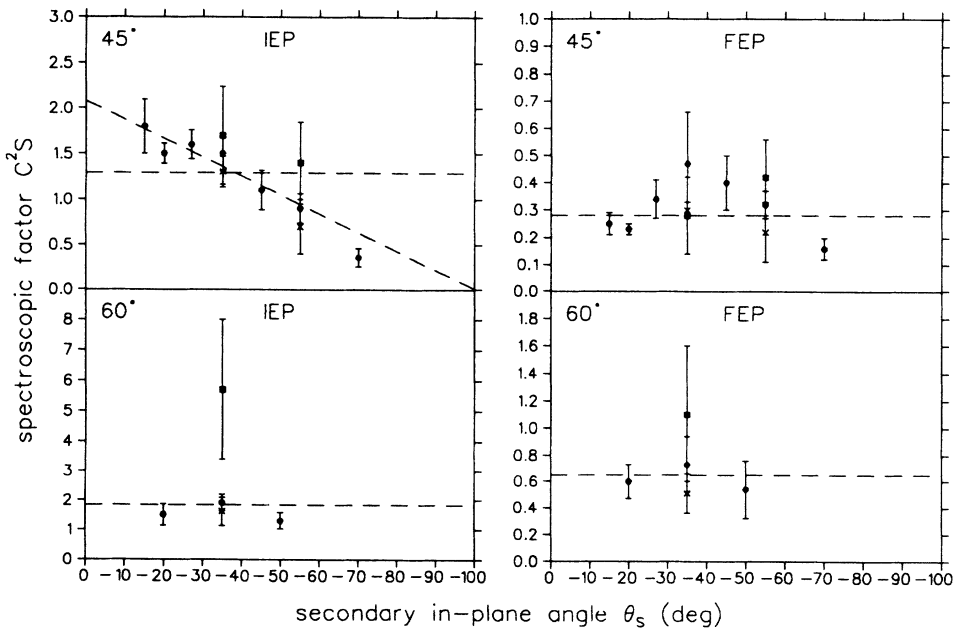


FIG. 9. Spectroscopic factors for (p,pd) at primary angles 45° and 60° , for each of the two prescriptions (as indicated). Other details are as given in Fig. 6.

($45^\circ; -65^\circ; 0^\circ$) (the calculation extends to np relative energies of 5 MeV, which can still be safely considered⁵⁵ as purely s -wave scattering). The calculated spectrum has been normalized to the peak in the data, and, when it is added incoherently to the DWIA calculation for the quasifree scattering, the overall agreement with the data is very good.

F. Sensitivity to the distorting potentials and bound-state wave function

The DWIA calculations are insensitive to the potential used for the incoming wave; a simultaneous change in all the well depths of 25% hardly affects the shapes of the energy-sharing distributions, and changes the magnitudes

by only 10–30%.

The outgoing distorted waves for the $(p, 2p)$ reaction do indicate some sensitivity to the well depths of the $p+t$ optical potentials (see Fig. 14): At the quasifree angle ($45^\circ; -27^\circ; 0^\circ$), a simultaneous reduction of V , W , V_{SO} , W_{SO} , and V_{ex} by 25% in both exit channels (which is possibly unreasonably large) causes the peak to broaden, and to shift downwards in primary proton energy by ~ 5 MeV (dashed curve) in addition to the 50% increase in overall magnitude which is reflected in the spectroscopic factors C^2S . The shift in the peak position is consistent with the investigations of Kroll and Wall⁵⁶ for changes in the strength of the real potentials; they found that the sensitivity to the imaginary potentials was limited to changes in absolute magnitude. Further investiga-

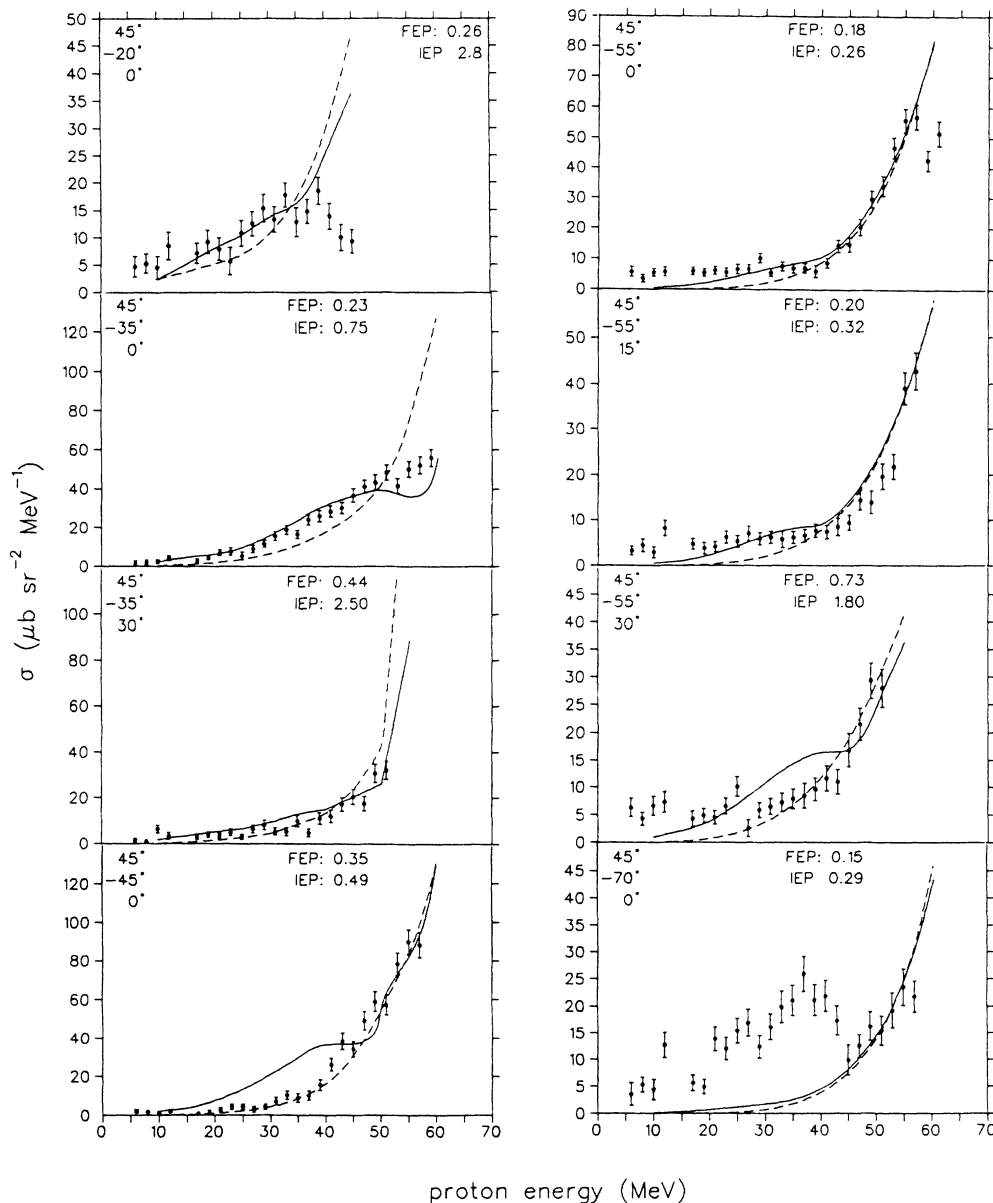


FIG. 10. Experimental cross sections and DWIA calculations for the quasifree knockout reaction ${}^4\text{He}(p,pt){}^1\text{H}$ at primary angle $\theta_p = 45^\circ$. See caption to Fig. 4.

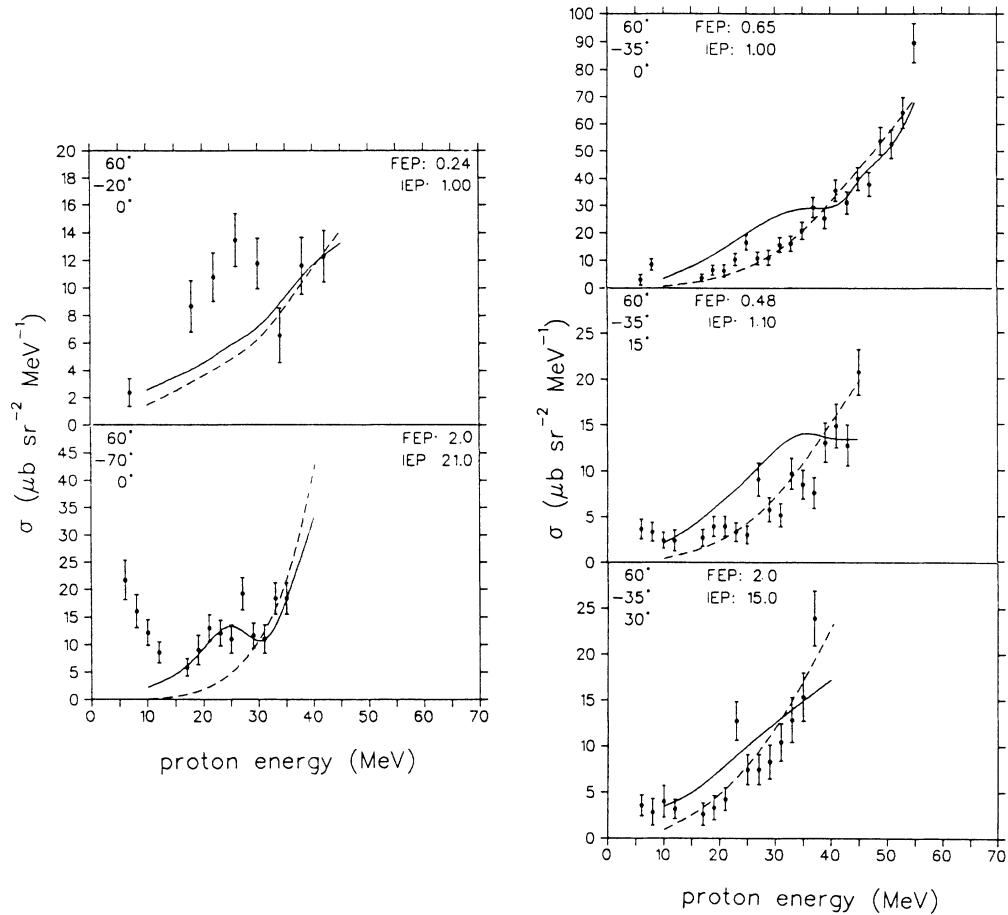


FIG. 11. Experimental cross sections and DWIA calculations for the quasifree knockout reaction ${}^4\text{He}(p,pt){}^1\text{H}$ at primary angle $\theta_p = 60^\circ$. See caption to Fig. 4.

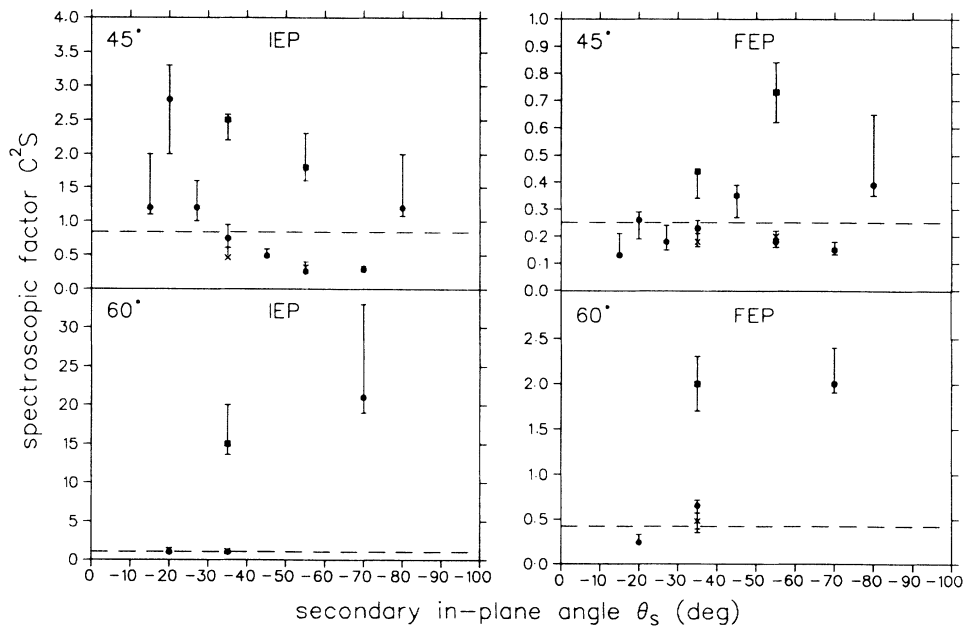


FIG. 12. Spectroscopic factors for (p,pt) at primary angles 45° and 60° , for each of the two prescriptions (as indicated). Other details are as given in Fig. 6.

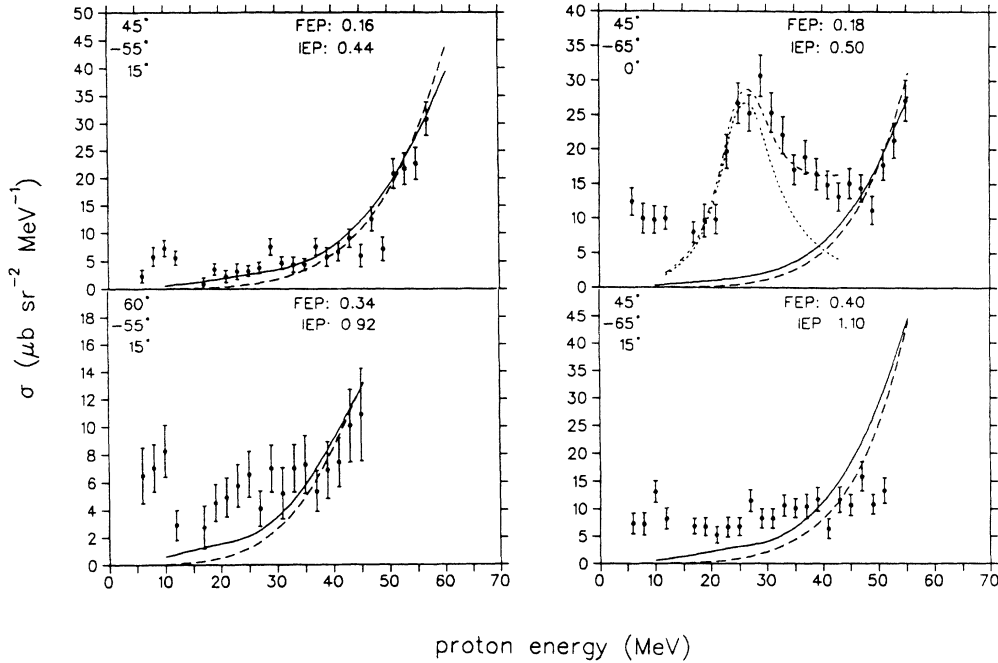


FIG. 13. Experimental cross sections and DWIA calculations for the quasifree knockout reaction ${}^4\text{He}(p,ph)n$. See caption to Fig. 4. At $(45^\circ; -65^\circ; 0^\circ)$, the final state interactions are fitted with a Watson-Migdal calculation (dotted curve). The dash-dotted curve represents the sum of the Watson-Migdal and FEP curves.

tion of this shape sensitivity confirms that the turnout in the distributions towards either end of the energy scale is an artefact of the energy-dependent potential breaking down for the outgoing proton with low energy. The distribution calculated with potentials fixed at an average energy of 40 MeV (dotted line) is better behaved at the extremes, but does not fit the data as well as does the energy-dependent calculation in the more important peak region.

At large secondary angles, on the other hand, there is minimal change in shape, and only a 20% change in magnitude when the outgoing potentials are changed in the same way. The calculations also seem to be less sensitive to the $p+d$ and $d+d$ potentials of the (p,pd) reaction. Even the magnitudes barely change.

The sensitivity of the $(p,2p)$ calculation to the bound-state wave function is shown in Fig. 15. There are minimal differences in shape between calculations with

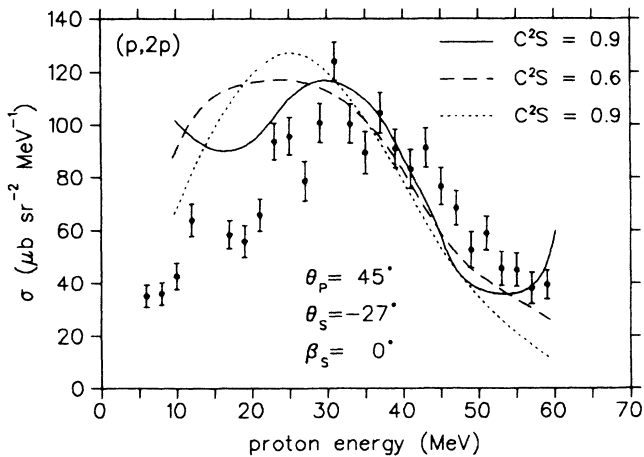


FIG. 14. Sensitivity to the optical potentials in the exit channels for $(p,2p)$. The solid curve represents our standard FEP calculation. The dashed curve is the result of changing the well depths by 25%, and is renormalized as indicated. The dotted curve is the result of using average-energy potentials.

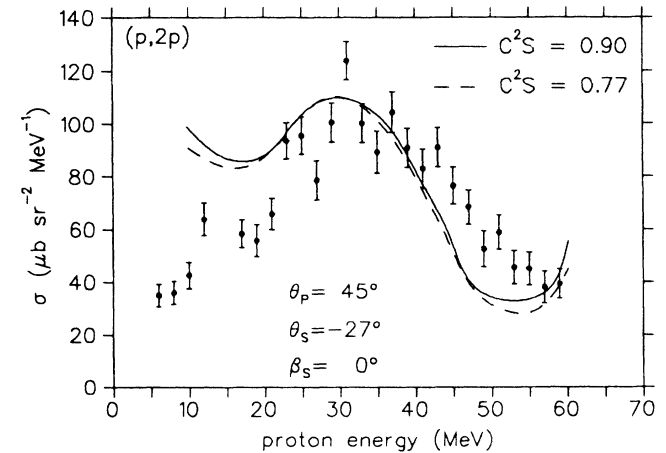


FIG. 15. Sensitivity of the $(p,2p)$ calculations to the bound-state wave function. The solid curve represents the FEP calculation with the wave function of van Oers *et al.* (Ref. 37). The dashed curve is for the parametrization of Lim (Ref. 44), renormalized as indicated.

the wave function of van Oers *et al.*,³⁷ and with that of Lim,⁴⁴ which is not surprising, because van Oers *et al.* noticed a difference only at high momenta (>400 MeV/ c). The use of Lim's parametrization increases the magnitude (i.e., reduces the spectroscopic factor) by 15% at the quasifree angle.

G. Corrections to the DWIA

It has been shown theoretically¹¹ that the effect of spin-orbit interactions on the DWIA cross sections could in principle be important. With the advent of the program THREEDDEE,³¹ which makes provision for spin-orbit terms in the optical potentials, several authors^{18,33,37,57,58} have investigated the sensitivity of their calculated DWIA cross sections to these interactions, with diverse results. It seems that one can expect normalizations to change by about 10–30%, but the direction of the change is unpredictable. The effects are not as a rule limited to regions of high recoil momenta, as was found³⁷ in the specific case of ${}^4\text{He}(p,2p)$ at ≥ 250 MeV. We find that the effect of turning off the spin-orbit terms in the potentials is to increase the calculated cross sections at the peak by $\sim 20\%$ for the $(p,2p)$ quasifree angle (see Fig. 16) and by $\sim 10\%$ for $(45^\circ; -70^\circ; 0^\circ)$. The changes in shape and magnitude agree with the findings of Chant and Roos³⁴ for $(p,2p)$ energy-sharing distributions from $l=0$ transitions.

Figure 17 shows the effect of turning off the corrections for the nonlocality of the optical potentials, at the $(p,2p)$ quasifree angle $(45^\circ; -27^\circ; 0^\circ)$. The turnout at the extremes is exacerbated, but the magnitude is hardly affected, whereas at large secondary angles the magnitude increases $\sim 20\%$, accompanied by slight shape differences. For (p,pd) the effect on both magnitude and shape is small. Thus the calculations do not seem to display great sensitivity to the nonlocality of the optical potentials, which was also the conclusion of van Oers *et al.*³⁷ for ${}^4\text{He}(p,2p)$ at 250, 350, and 500 MeV.

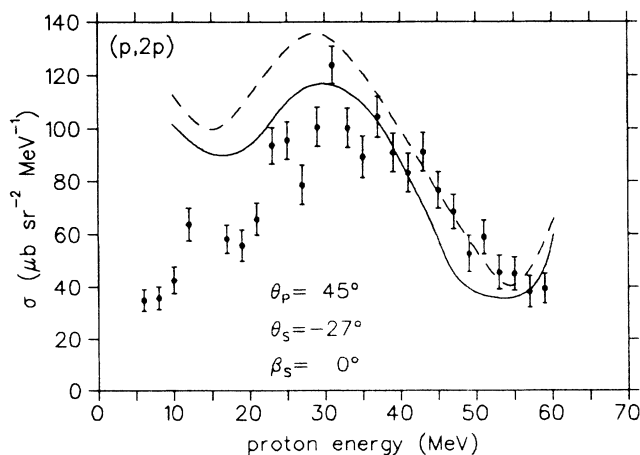


FIG. 16. The effect of turning off the spin-orbit terms in the optical potentials. The solid curve represents the standard FEP calculation with the full spin-orbit potentials. The dashed curve is for no spin-orbit terms.

H. Applicability of the DWIA

The DWIA does quite well in modeling the quasifree knockout of protons from ${}^4\text{He}$, although there are minor problems at the extreme ends of the primary proton energy scale, particularly for forward angles of the coincident secondary proton. For the knockout of deuterons, the calculations give a reasonable fit to the data (in terms of shape), but underestimate the high-energy yields at many of the coincidence angles. On the other hand, for triton and helion knockout, it is the calculation which rises somewhat more rapidly than the data towards high primary proton energy, although the overall fits are still reasonable.

In general we have demonstrated empirically that the DWIA is applicable to the reaction ${}^4\text{He}(p,p'x)$ at 100 MeV over most of the phase space containing the major yield. There are, however, a number of approximations in the theory which might be significant^{18,32,36,59,60} for these reactions. Therefore, it would be unwise to extend these calculations to geometries far from those which have been tested here.

I. Angle-dependent spectroscopic factors

For ${}^4\text{He}(p,2p)$, the angle dependence of the extracted spectroscopic factors is pronounced: For example, we see an increase of a factor of 3–4 (see Fig. 6) between the quasifree angle $(45^\circ; -27^\circ)$ and the largest angle measured $(45^\circ; -90^\circ)$. A similar trend is found⁵⁸ for ${}^{12}\text{C}(p,2p)$ at 200 MeV; and for the same reaction at 100 MeV, Devins *et al.*⁶¹ find that the spectroscopic factor derived from angular correlation data at symmetric angles is double that derived from data at asymmetric angles.

This angle-dependent trend is also a feature of comparisons between DWIA calculations and inclusive (p,p') measurements. Wesick *et al.*¹⁸ see a factor of 3–6 increase (depending on the prescription used for the two-body interaction) in the spectroscopic factor between

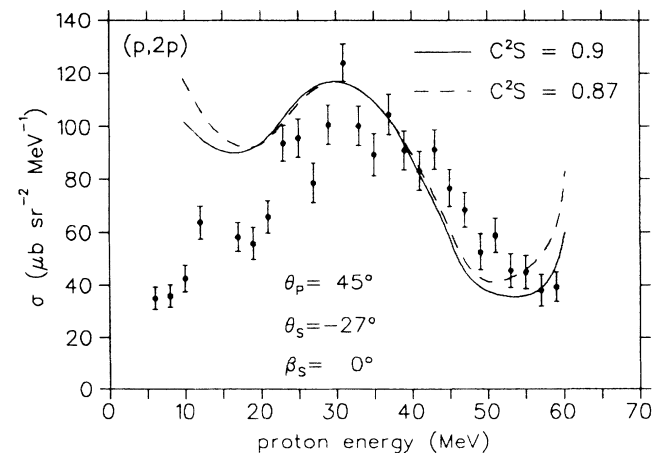


FIG. 17. The effect of turning off the corrections for nonlocality in the optical potentials. The solid curve represents the FEP calculation with nonlocality corrections. The dashed curve is for no nonlocality corrections, and is renormalized as indicated.

17.5° and 60°, for ${}^4\text{He}(p,p')$ at 100 MeV. For ${}^{12}\text{C}(p,p')$ at 90 and 200 MeV, Förtsch *et al.*¹⁶ find a similar trend with increasing scattering angle, although the angle dependence is less severe.

Inspection of the least-squares fits to the $(p,2p)$ spectroscopic factors shown in Fig. 6 reveals that the angle dependence has roughly the same slope for $\theta_p=45^\circ$ and 60° . Furthermore, the offset between the two sets is close to 15° , which is the difference between the two primary angles. Thus the physics behind the angle dependence appears to be related to the separation angle $\theta_p - \theta_S$.

As the bulk of the coincidence yield for $\theta_p=60^\circ$ is biased towards larger separation angles, where the spectroscopic factors are higher, it is evident that the inclusive cross section, i.e., the integrated coincidence yield, as measured by Wesick *et al.*, will require a larger spectroscopic factor to normalize the DWIA calculation at 60° than at 45° . Consequently we propose that the angle dependence of the spectroscopic factors in the inclusive calculations of Wesick *et al.*, and in the exclusive calculations of this work, have their origin in one and the same phenomenon, which is a dependence on the separation angle $\theta_p - \theta_S$. This in turn is suggestive of a dependence on a quantity such as the recoil momentum. From an investigation of the angle dependence of the various factors which comprise the DWIA cross section [Eq. (6)], we conclude that the angle dependence of the spectroscopic factors suggests a discrepancy between the data and the calculated distorted momentum distribution. Our results show that generally the DWIA falls off too rapidly with respect to the data beyond ~ 100 MeV/ c . Thus the increasing trend in the spectroscopic factors towards large angles is possibly a consequence of these angles being sensitive to only the higher-momentum components of the bound-state wave function.

Larger than expected high-momentum components have been seen in almost all other measurements^{21,22,37,62} of ${}^4\text{He}(p,2p)$. A number of possible explanations³⁷ have been put forward for the enhanced contributions to the data at high recoil momenta (approximately a factor of 2 at 200 MeV/ c). Apart from general flaws in the DWIA description of the reaction, such as the inadequacy of the optical potentials and the bound-state wave function, the most likely cause would seem to be that other mechanisms, which are not accounted for in the DWIA, manifest themselves at high momenta, where the DWIA cross section becomes small. Several rescattering and exchange terms have been proposed.³⁷

In conclusion, we speculate that the origin of the angle-dependent spectroscopic factors is traceable to an inability of the DWIA to reproduce the high-momentum components of the distorted momentum distribution. Although the reason for this failure cannot be pinpointed with certainty, it is suspected that contributions from other diagrams might constitute the remainder of the yield at these momenta.

VI. RECONSTRUCTING THE INCLUSIVE SPECTRA

A. Quasifree knockout

We have shown that the DWIA is capable of describing the quasifree mechanism adequately for all possible

knocked-out particles from ${}^4\text{He}$ (except for neutrons, which have not been investigated) over the solid angle range of major yield. Having extracted spectroscopic factors for each reaction type, we may now determine the total contribution of quasifree knockout to the inclusive yield simply by integrating the coincidence cross sections over the solid angles of the various secondary particles [Eq. (7)].

As pointed out by Wesick *et al.*,¹⁸ there is some ambiguity in how one should treat the distortion of the (now unobserved) secondary particle. As the inclusive cross section depends only on the primary proton emerging cleanly from the nucleus, it does not matter whether the secondary particle is subsequently rescattered or even absorbed.⁵⁶ Thus the use of a complex optical potential to distort the outgoing wave function is inappropriate, and one should use either a plane wave or at most a purely real potential. Although it has been suggested⁶³ that the purely real potential is more consistent theoretically, we have chosen to use plane waves for the undetected particle. We have followed Wesick *et al.*¹⁸ in using n - n rather than p - p phase shifts for the two-body t matrix in the (p,p') calculations, as they found that the Coulomb interaction caused unphysical spikes in the integrated yield. The neglect of this long-range interaction is justified on the grounds that the impulse approximation describes essentially a short-range mechanism.

We integrated between solid angle endpoints which encompassed all that phase space for which recoils of < 200 MeV/ c were possible (see Fig. 2), except that the integrations were truncated at $\theta_S=0^\circ$, because of a suspected breakdown in the DWIA at positive secondary angles.⁶⁴ This causes the integrated yields to be only slightly underestimated, as the major part of the yield is concentrated around low recoil momenta on the opposite side of the beam from the primary telescope. For the (p,pn) calculations, the spectroscopic factors were assumed to be the same as for $(p,2p)$.

The results of calculations in which angle-averaged spectroscopic factors were used are shown in Figs. 18 and 19 for $\theta_p=45^\circ$ and 60° , respectively. The curve labeled "Sum" represents the sum of the calculated contributions from the quasifree knockout of protons, neutrons, deuterons, tritons, and helions, added incoherently. At 45° the IEP calculation accounts for $\sim 60\%$ of the inclusive yield between 10 and 55 MeV, and the FEP $\sim 80\%$. The difference stems mainly from the (p,pn) contribution, for which spectroscopic factors might not be accurate. Another discrepancy is in the contribution from triton and helion knockout at high energy of the primary proton, which reflects uncertainties in the two-body t matrix (off-shell effects combined with interpolation errors in sparse elastic scattering data). Nevertheless, for both prescriptions it is clear that most of the quasifree knockout contribution at high energy is in the form of cluster knockout, confirming the speculations of Wesick *et al.* For $\theta_p=60^\circ$ the result is similar, with the total estimated contribution from quasifree knockout being $\sim 60\%$ (IEP) or $\sim 70\%$ (FEP) of the experimentally measured yield.

Although we showed in Sec. V E that the effect of final

state interactions could be significant at certain coincidence geometries, their estimated contributions to the integrated yield are insignificant over the energy region being studied (10 to 55 MeV), and may consequently be neglected in these calculations.

The comparison of the $(p,2p)$ calculations with constant, or angle-dependent spectroscopic factors is shown for $\theta_p=45^\circ$ in Fig. 20, indicating shape changes in the 10–30% range. It might seem surprising that the difference is not more profound, as the spectroscopic factors change by about a factor of 3 between $\theta_S=-15^\circ$ and -90° . However, this relative insensitivity is a consequence of the major yield being concentrated into a fairly small region of laboratory coordinate space. For $\theta_p=45^\circ$, for instance, most of the cross section comes from secondary protons emitted with laboratory angles between -25° and -55° . Over this range, the least-squares constant spectroscopic factor is not very different from the linearly dependent fit (see Fig. 6).

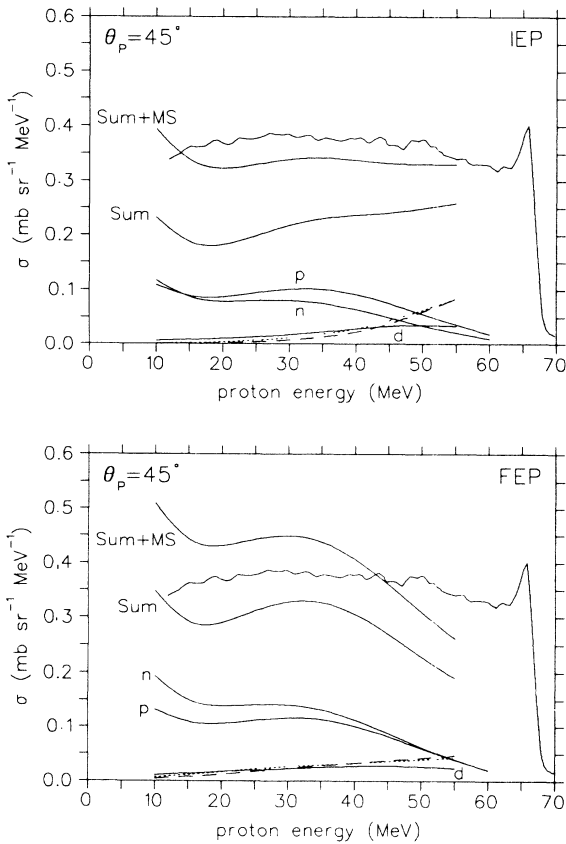


FIG. 18. Calculations of inclusive cross sections at 45° , compared with the data of Wesick *et al.* (Ref. 18), for the IEP (above) and the FEP (below). The curve labeled “Sum” represents the sum of the contributions from the quasifree knockout of protons (“p”), neutrons (“n”), deuterons (“d”), tritons (dashed), and helions (dotted). “Sum+MS” includes the estimated contribution from multiple scattering, added incoherently to the quasifree contributions.

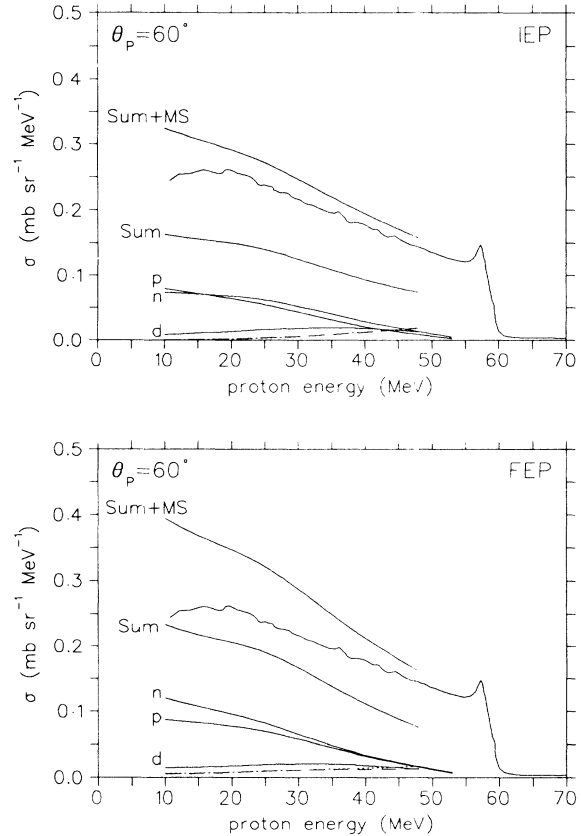


FIG. 19. Calculations of inclusive cross sections at 60° , compared with the data of Wesick *et al.* (Ref. 18), for the IEP (above) and the FEP (below). The curves are labeled as in Fig. 18.

B. Multiple scattering

We have shown above that the total contribution of quasifree knockout to the inclusive continuum yields is between 60% and 80%. All the other reaction channels, which mainly involve direct breakup, or the excitation of the residual nucleus (leading to sequential decay), are

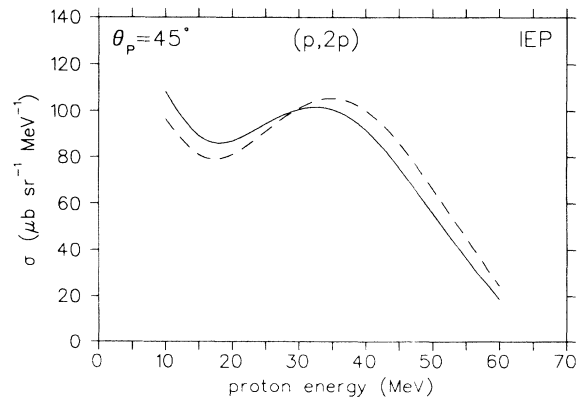


FIG. 20. A comparison between the angle-integrated $(p,2p)$ yields at 45° , calculated for a constant spectroscopic factor (solid curve), and for angle-dependent spectroscopic factors (dashed curve).

loosely called “multiple scattering.”

In order to test whether multiple scattering would fill in the remainder of the yield, we made a crude estimate of this contribution, based on our data outside the quasi-free kinematic locus. First, we assumed that the average proton multiplicity was approximately 2, i.e., the primary proton was emitted along with one other proton (on average) from the various breakup channels. Secondly, the breakup of the target was assumed to arise from either an initial quasifree scattering, followed by further collisions with the recoiling spectator, or from “other mechanisms.” Now the former mechanism has already been partially included in the calculated inclusive yields by our taking plane waves for the unobserved particle in the integration over solid angle, which thus allows for multiple scattering of this particle too. If we think of this quasi-free doorway mode in terms of the Ciangaru picture,⁶⁵ which treats the struck nucleon as an intranuclear projectile scattering inelastically off the residual nucleus, then it is clear that such a multiple scattering component will be forward peaked. However, the “other mechanisms” which still need to be included are assumed to be isotropic in phase space. Thus, to select only these contributions, we took the multiple scattering yield at relatively backward coincidence angles [(45°; -80°; 0°) and (60°; -70°; 0°)] and integrated it over phase space. Quite coincidentally, the results of these estimates for $\theta_p = 45^\circ$ and for $\theta_p = 60^\circ$ were identical:

$$\frac{d^2\sigma}{d\Omega_p dE_p} = (0.181 - 0.002T_p) \text{ mb sr}^{-1} \text{ MeV}^{-1}. \quad (9)$$

The incoherent sum of this estimated multiple scattering contribution and the quasifree knockout cross sections is shown as the upper curve (“Sum+MS”) in Figs. 18 and 19.

C. Discussion

In order to compare the quality and consistency of the final results for the various prescriptions and spectroscopic factor dependences, we have renormalized them to the inclusive data for presentation in Fig. 21, and normalization factors are given in Table III.

At 45° the IEP reproduces the flat continuum spectrum better than the FEP, although it overestimates the low-energy portion. The FEP curves both underpredict the high-energy portion of the spectrum. In this instance, the use of angle-dependent spectroscopic factors (dotted curve) does improve the quality of the fit somewhat. For both the constant and the angle-dependent spectroscopic factors, the IEP curves were $\sim 10\%$ low before renormalization, and the FEP curves were $\sim 10\%$ high. The difference stems from the total quasifree knockout contributions being calculated as 60% for the IEP and 80% for the FEP (between 10 and ~ 50 MeV). Thus if we consider the two prescriptions as delimiting the uncertainty in the on-shell treatment of the two-body t matrices, then the experimental spectrum lies squarely on the average of the two, with a $(70 \pm 10)\%$ contribution from quasifree knockout and a $(30 \pm 10)\%$ contribution from multiple scattering.

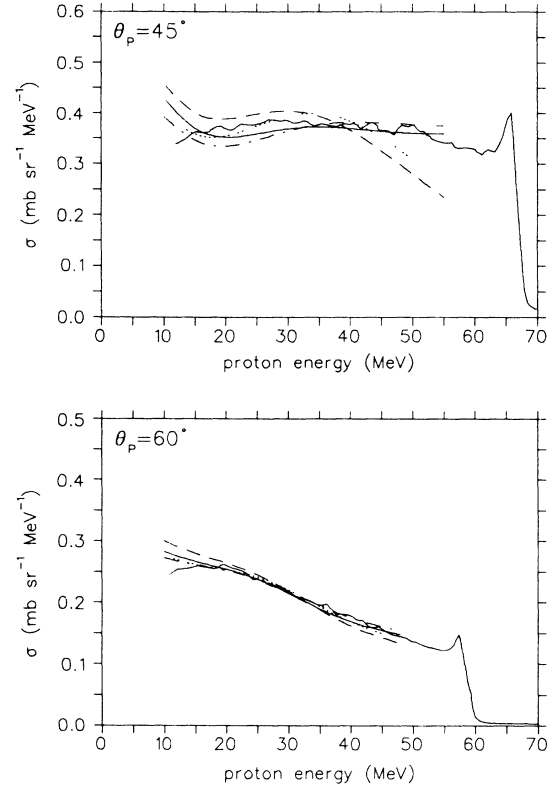


FIG. 21. Comparisons of the calculated inclusive cross sections at 45° (above) and 60° (below). The curves are normalized to the experimental data with the factors given in Table III, and represent the sum of all the quasifree knockout contributions and the estimated multiple scattering contribution, as follows: Solid curve: IEP with constant spectroscopic factors C^2S . Dash-dotted curve: IEP with angle-dependent C^2S . Dashed curve; FEP with constant C^2S . Dotted curve: FEP with angle-dependent C^2S .

At 60° the slope of the experimental distribution is reproduced almost exactly by both prescriptions with both methods of treating the spectroscopic factors, except at the lowest energies, where they fail to turn down as the data do. All the calculations overpredict the total yield, however, and need to be renormalized by between

TABLE III. Normalization factors for the calculated inclusive cross sections shown in Fig. 21. At each angle the IEP and FEP on-shell approximations (OSA) are calculated with both constant spectroscopic factors C^2S and angle-dependent spectroscopic factors (for the nucleon-knockout component).

Angle	OSA	C^2S	Factor
45°	IEP	Constant	1.09
		Ang.-dep.	1.09
	FEP	Constant	0.90
		Ang.-dep.	0.93
60°	IEP	Constant	0.87
		Ang.-dep.	0.90
	FEP	Constant	0.76
		Ang.-dep.	0.81

10% and 25% to give the agreement as shown. The IEP (FEP) gives the quasifree knockout component as 60% (70%) of the total yield, which is consistent with the $(70\pm 10)\%$ extracted from the comparisons at 45° . This implies that the multiple scattering contribution is 30–40%, instead of $\sim 60\%$ as estimated in Sec. VIB (from a rough analysis of the coincidence data below the quasifree locus). We do not think that much importance should be attached to this discrepancy, in the light of the crudeness of the latter estimate.

For both primary angles, $\sim 75\%$ of the quasifree component comes from nucleon knockout and the rest comes from cluster knockout. At 10 MeV, the (p,pN) contribution is over 90%, whereas at the highest energies it is only 20–40%, with the bulk of the quasifree yield coming from the knockout of deuterons, tritons, and helions.

The lack of a visible quasifree peak, which bothered Wesick *et al.*,¹⁸ is seen to have a simple explanation: The (p,pN) distribution does indeed have a maximum (at ~ 30 MeV for $\theta_p=45^\circ$, see Fig. 18), but this is washed out by the cluster knockout contributions picking up towards higher energies of the primary proton. Although some semblance of this peak remains in the FEP curve, it disappears altogether in the IEP prediction. Thus the lack of a quasifree peak does not necessarily imply that the reaction mechanism is dominated by multiple scattering. The fact that the measured spectrum at 45° continues without dropping (beyond the high-energy cutoff of these calculations) may well be caused by the excitation of high-lying unbound states in ${}^4\text{He}$, as suggested by Wesick *et al.*

Most of the uncertainty in the estimated shape and magnitude of the inclusive quasifree scattering component arises from two sources: The spectroscopic factors for the (p,pn) contributions, and the high-energy cluster knockout contributions. We justify using the $(p,2p)$ spectroscopic factors for (p,pn) also (on the self-conjugate target ${}^4\text{He}$), on the basis of the arguments put forward by Kitching *et al.*,⁶⁰ who claim that all the factors [Eq. (6)] in the DWIA cross section for the two reactions should be about the same, except for the free N - N cross section, which is, of course, treated properly in THREEDDEE.³¹ Other differences would depend on the bound-state wave functions for the proton or the neutron, and on the different optical potentials for scattering off the mirror residual nuclei. We have seen in Sec. IV that the bound-state wave function is taken to be the same for the proton or the neutron in ${}^4\text{He}$, as isospin invariance was assumed in its derivation. It is argued⁶⁰ that the effect of the small difference in binding energy is essentially cancelled by the Coulomb force suppressing the tail of the proton wave function. Similarly, as discussed in Sec. IV, the same optical potential was used for the distortions in the final states of the (p,pn) reaction as was used for $p+{}^3\text{H}$ in the $(p,2p)$ reaction, since the isospin coupling was found³⁷ to be weak.

The other major source of uncertainty, namely fitting the high-energy portion of the (p,pt) and (p,ph) distributions, manifests itself in the divergent shapes of the IEP and FEP integrated yields at high energies of the primary proton (see Fig. 21). It would not be a simple matter to

remedy this situation. First, there is the difficulty of normalizing the calculated DWIA curves to the steeply rising knockout data. Then there is the sparseness of the elastic scattering data which introduces large uncertainties in the two-body cross sections for each on-shell prescription. Finally, it is probable^{18,60} that other approximations in the DWIA require careful scrutiny in the case of cluster knockout from a light nucleus. Fortunately, these uncertainties are not so large as to challenge the broad conclusions which we have made, although they do prevent an accurate estimate of the proportion of quasifree scattering in the total yield.

It is interesting to make a rough comparison between our results on ${}^4\text{He}$ and the predictions of some preequilibrium models for heavier targets. All of these models, whether semiclassical or quantum mechanical, compute the continuum spectrum as arising from a series of N - N interactions, with a certain probability of emission after each step, so the probability for quasifree scattering is obtained simply by truncating the series after one step. Our results thus represent a semiempirical determination of the fraction of the yield attributable to the first step.

Chiang and Hüfner⁷ have developed a simple theory which allows the calculation of continuum spectra from the sum of just three terms, representing single scattering, double scattering, and compound nucleus formation, respectively. Despite the unsophisticated approach, these calculations have been reasonably successful in fitting inclusive continuum spectra generated by 15–100 MeV incident protons and neutrons on a range of targets from ${}^{12}\text{C}$ to ${}^{209}\text{Bi}$ (in some cases doing better than the more complicated exciton model). Chiang and Hüfner conclude that single scattering dominates the cross section except at large energy losses, where multistep mechanisms take over, as one might expect. For instance, they estimate that for mean free paths in the range 3–5 fm (the upper limit is probably most appropriate⁶⁶ for 100 MeV incident energies), the proportion of quasifree scattering in the total yields is 60–70% for a ${}^{12}\text{C}$ target, 50–60% for ${}^{54}\text{Fe}$, and 30–40% for ${}^{209}\text{Bi}$. These estimates seem a little high in the light of our estimate of $(70\pm 10)\%$ for the very light nucleus ${}^4\text{He}$.

Recently, Smith and Bozoian⁶⁷ have taken a similar approach, which was first proposed by Wu.⁶⁸ They replace the first step of the exciton model calculation (the $2p1h$ term) by an explicit calculation for quasifree scattering, while the multiple scattering contribution is calculated in the normal way by the exciton model, from the $3p2h$ term onwards. The quasifree scattering is calculated in a Fermi-gas model for the nuclear response function, with the absorption being given by a modified Glauber theory. The calculation is renormalized to yield the correct reaction cross section by modifying only the depletion factors in the exciton part of the series.

From the results of these calculations, it is claimed that the quasifree term dominates the inclusive continuum yields from various nuclei at incident energies between 60 and 200 MeV. For instance the proportion of quasifree scattering from ${}^{27}\text{Al}$ at 90 MeV is claimed to be 70%, and for ${}^{54}\text{Fe}$ at 62 MeV it is $\sim 60\%$, which again is somewhat higher than might be expected from our results. Howev-

er, the fits to the data are generally not good, and it thus seems difficult to justify the way in which the calculations were renormalized, where it was assumed that the absolute magnitude of the quasifree part was correct.

VII. SUMMARY AND CONCLUSIONS

Exclusive measurements have been made of the reactions ${}^4\text{He}(p,2p)$, (p,pd) , (p,pt) , and (p,ph) at 100 MeV. The primary protons were measured at two angles, 45° and 60°, in coincidence with secondary protons, deuterons, tritons, or helions at secondary angles ranging from -15° to -90° in plane, and from 0° to 30° out of plane.

For the $(p,2p)$ reaction, the comparison between the experimental data and the curves calculated by means of the DWIA is satisfactory over the entire solid angle range of the energy-sharing distributions. However, the DWIA results tend to turn upwards at the extremes of the energy scale, particularly at forward angles, which is a trend not reflected in the experimental data. The spectroscopic factors which are required to normalize the DWIA curves to the experimental energy-sharing distributions are angle dependent, with an increasing trend towards larger secondary angles.

The DWIA calculations for the (p,pd) reaction are in reasonable agreement with the data, although they are not as good as for proton knockout. There are bigger differences between the curves for the two on-shell prescriptions, and the spectroscopic factors are not as systematic as for $(p,2p)$. They are reasonably constant with angle, however, except for the IEP at primary proton angle 45°, which tends to decrease towards larger secondary angles.

For the (p,pt) and (p,ph) reactions, the DWIA curves are in reasonable agreement with the data from secondary angles of -35° outwards, but at forward angles the agreement is poor. There are large uncertainties in the extracted spectroscopic factors because of the difficulty in normalizing the curves to the data, which rise steeply towards the high-energy cutoff of the energy-sharing distributions. At some angles, the data indicate strong contributions from final state interactions. A Watson-Migdal calculation of the final state interaction was added incoherently to the DWIA results and gave good overall agreement with these experimental distributions.

The sensitivity of the DWIA calculations to details of the distorting potentials was investigated. It was found that the calculations were not sensitive to the optical potential in the entrance channel, but that there was some sensitivity in predicted magnitude and peak position to changes in the outgoing potentials for the $(p,2p)$ reaction. The cluster knockout calculations are not as sensitive to the potentials in the exit channel. Furthermore, the calculations are not very sensitive to details of the bound-state wave functions. The nonlocality corrections changed some of the cross sections by $\sim 20\%$, and the effect of the spin-orbit interactions in the optical potentials was found to vary with angle from 3% to 20%.

The angle dependence of the spectroscopic factors probably results from an inability of the DWIA to reproduce the high-momentum components of the distorted

momentum distribution. This also provides a ready explanation of the angle dependence found by Wesick *et al.*¹⁸ in the inclusive measurements. It is suspected that the extra yield at high momenta is the result of contributions from mechanisms not described in the DWIA.

Despite theoretical misgivings about applying distorted-wave techniques to light systems, it is concluded that the DWIA is an adequate formalism for modeling the quasifree knockout reactions induced by 100 MeV protons on ${}^4\text{He}$. Although there were indications that the model was starting to break down under extreme kinematic conditions, it nevertheless gave a reasonable description of the various knockout cross sections over the range of major yield.

Consequently, it was appropriate to calculate the quasifree knockout contribution to the inclusive spectra, by integrating the DWIA cross sections over the solid angles of the secondary particles, using the average spectroscopic factors extracted from the coincidence data. For the (p,pn) reaction, it was assumed that the spectroscopic factors were the same as for $(p,2p)$. A comparison of these calculations with the inclusive spectra measured by Wesick *et al.* reveals that quasifree scattering accounts for 60–80% of the yield at 45°, and 60–70% at 60°. Improved calculations which allow for the angle dependence of the spectroscopic factors give similar results. The major sources of uncertainty in these calculations are the spectroscopic factors for neutron knockout, and the cluster knockout contributions at high energies of the scattered proton.

At low energies of the scattered proton (~ 10 MeV), more than 90% of the quasifree yield comes from nucleon knockout, whereas at higher energies, it is the knockout of deuterons, tritons, and helions which contributes most of the yield. A rough estimate of the multiple scattering yield was made from a further analysis of the coincidence data. When this is added to the quasifree component, the measured inclusive yield at 45° is reproduced to within 10%, but the yield at 60° is overestimated by 10–25%. At 45° the flat shape of the inclusive spectrum is well reproduced by the DWIA calculations with the initial-energy prescription (IEP) plus the estimated multiple scattering component. The lack of a discernible quasifree peak is seen to arise from the superposition of the cluster knockout contributions on the high-energy side of the quasifree nucleon-knockout peak. Thus we have shown that the featureless inclusive spectra from ${}^4\text{He}(p,p')$ at 45° and 60° are compatible with the interpretation of a reaction mechanism dominated by quasifree scattering.

Finally, we summarize the principal conclusions of this work as follows:

- (1) The DWIA is an appropriate formalism for modeling the quasifree knockout reactions ${}^4\text{He}(p,p'x)$ at 100 MeV, over a wide kinematic range.
- (2) The continuum ${}^4\text{He}(p,p')$ cross sections at 45° and 60° are dominated by quasifree scattering ($\sim 70\%$), with $\sim 30\%$ arising from multiple scattering.
- (3) The contribution of cluster knockout to the inclusive yields is significant. Although nucleon knockout constitutes over 90% of the quasifree component at 10

MeV, at high energies of the scattered proton it makes up only 20–40% of the quasifree yield, with the balance coming from the knockout of deuterons, tritons, and helions.

(4) The absence of discernible quasifree peaks in the inclusive spectra is probably due to the cluster knockout contributions filling in the yield at higher energies.

(5) The angle dependences of the spectroscopic factors for both the inclusive (p, p') and the exclusive ($p, 2p$) cal-

culations may be due to the DWIA underpredicting the wings of the distorted momentum distribution.

ACKNOWLEDGMENTS

We thank Professor P. G. Roos for a critical appraisal of the manuscript. The assistance of C. J. Stevens and V. C. Wikner is gratefully acknowledged.

- ¹See, e.g., Josef Speth and Adriaan van der Woude, *Rep. Prog. Phys.* **44**, 719 (1981).
- ²See, e.g., H. Gruppelaar, P. Nagel, and P. E. Hodgson, *Riv. Nuovo Cimento* **9**, 1 (1986).
- ³J. J. Griffin, *Phys. Rev. Lett.* **17**, 478 (1966).
- ⁴Marshall Blann, *Phys. Rev. Lett.* **28**, 757 (1972).
- ⁵Herman Feshbach, Arthur Kerman, and Steven Koonin, *Ann. Phys. (N.Y.)* **125**, 429 (1980).
- ⁶M. Blann, *Nucl. Phys.* **A213**, 570 (1973).
- ⁷H. C. Chiang and J. Hüfner, *Nucl. Phys.* **A349**, 466 (1980).
- ⁸M. Trabandt, W. Scobel, M. Blann, B. A. Pohl, R. C. Byrd, C. C. Foster, and R. Bonetti, *Phys. Rev. C* **39**, 452 (1989); W. Scobel, M. Trabandt, M. Blann, B. A. Pohl, B. R. Remington, R. C. Byrd, C. C. Foster, R. Bonetti, C. Chiesa, and S. M. Grimes, *ibid.* (to be published).
- ⁹Peter A. Wolff, *Phys. Rev.* **87**, 434 (1952).
- ¹⁰Daphne F. Jackson and Tore Berggren, *Nucl. Phys.* **62**, 353 (1965).
- ¹¹Daphne F. Jackson, *Nucl. Phys.* **A257**, 221 (1976).
- ¹²N. S. Wall and P. R. Roos, *Phys. Rev.* **150**, 811 (1966).
- ¹³R. E. Segel, T. Chen, L. L. Rutledge, Jr., J. V. Maher, John Wiggins, P. P. Singh, and P. T. Debevec, *Phys. Rev. C* **26**, 2424 (1982).
- ¹⁴R. E. Segel, S. M. Levenson, P. Zupranski, A. A. Hassan, S. Mukhopadhyay, and J. V. Maher, *Phys. Rev. C* **32**, 721 (1985).
- ¹⁵J. R. Wu, C. C. Chang, and H. D. Holmgren, *Phys. Rev. C* **19**, 698 (1979); A. A. Cowley, C. C. Chang, and H. D. Holmgren, *ibid.* **22**, 2633 (1980).
- ¹⁶S. V. Förtsch, A. A. Cowley, J. V. Pilcher, D. M. Whittal, J. J. Lawrie, J. C. van Staden, and E. Friedland, *Nucl. Phys.* **A485**, 258 (1988).
- ¹⁷F. E. Bertrand and R. W. Peelle, *Phys. Rev. C* **8**, 1045 (1973).
- ¹⁸J. S. Wesick, P. G. Roos, N. S. Chant, C. C. Chang, A. Nadasen, L. Rees, N. R. Yoder, A. A. Cowley, S. J. Mills, and W. W. Jacobs, *Phys. Rev. C* **32**, 1474 (1985).
- ¹⁹S. Fiarman and W. E. Meyerhof, *Nucl. Phys.* **A206**, 1 (1973).
- ²⁰K. Fukunaga, S. Kakigi, T. Ohsawa, A. Okihana, T. Sekioka, H. Nakamura-Yokota, and S. Tanaka, *Nucl. Phys.* **A456**, 48 (1986); L. C. Bland, J. Breeden, K. Murphy, W. W. Jacobs, B. Raue, J. Sowinski, J. Templon, S. Vigdor, and J. Wilkerson, *Indiana University Cyclotron Facility Newsletter* No. 40, 1987, p. 6.
- ²¹H. G. Pugh, P. G. Roos, A. A. Cowley, V. K. C. Cheng, and R. Woody, *Phys. Lett.* **46B**, 192 (1973).
- ²²R. Frascaria, P. G. Roos, M. Morlet, N. Marty, A. Willis, V. Comparat, and N. Fujiwara, *Phys. Rev. C* **12**, 243 (1975).
- ²³A. H. Botha, H. N. Jungwirth, J. J. Kritzinger, D. Reitmann, and S. Schneider, in *Proceedings of the Eleventh International Conference on Cyclotrons and their Applications, Tokyo, 1986*, edited by M. Sekiguchi, Y. Yano, and K. Hatanaka (Ionics Publishing Co., Tokyo, 1987), p. 9.
- ²⁴J. V. Pilcher, A. A. Cowley, D. M. Whittal, and J. J. Lawrie, *Phys. Rev. C* **40**, 1937 (1989).
- ²⁵T. A. Carey, Ph.D. thesis, University of Maryland, 1979.
- ²⁶J. B. Birks, *The Theory and Practice of Scintillation Counting* (Pergamon, Oxford, 1964), pp. 437–440.
- ²⁷R. J. Meijer, A. van den Brink, E. A. Bakkum, P. Decowski, K. A. Griffioen, and R. Kamermans, *Nucl. Instrum. Methods* **A256**, 521 (1987).
- ²⁸R. E. L. Green, D. H. Boal, R. L. Helmer, K. P. Jackson, and R. G. Korteling, *Nucl. Phys.* **A405**, 463 (1983).
- ²⁹J. M. Cameron, P. Kitching, R. H. McCamis, C. A. Miller, G. A. Moss, J. G. Rogers, G. Roy, A. W. Stetz, C. A. Goulding, and W. T. H. van Oers, *Nucl. Instrum. Methods* **143**, 399 (1977).
- ³⁰Joseph F. Janni, *At. Data Nucl. Data Tables* **27**, 147 (1982).
- ³¹N. S. Chant, Code THREEDDE, University of Maryland (unpublished).
- ³²N. S. Chant and P. G. Roos, *Phys. Rev. C* **15**, 57 (1977).
- ³³N. S. Chant, P. Kitching, P. G. Roos, and L. Antonuk, *Phys. Rev. Lett.* **43**, 495 (1979).
- ³⁴N. S. Chant and P. G. Roos, *Phys. Rev. C* **27**, 1060 (1983).
- ³⁵Gerhard Jacob and Th. A. J. Maris, *Rev. Mod. Phys.* **38**, 121 (1966).
- ³⁶Edward F. Redish, G. J. Stephenson, Jr., and Gerald M. Lerner, *Phys. Rev. C* **2**, 1665 (1970).
- ³⁷W. T. H. van Oers, B. T. Murdoch, B. K. S. Koene, D. K. Hasell, R. Abegg, D. J. Margaziotis, M. B. Epstein, G. A. Moss, L. G. Greeniaus, J. M. Greben, J. M. Cameron, J. G. Rogers, and A. W. Stetz, *Phys. Rev. C* **25**, 390 (1982).
- ³⁸F. Perey and B. Buck, *Nucl. Phys.* **32**, 353 (1962).
- ³⁹P. G. Roos, D. A. Goldberg, N. S. Chant, R. Woody, III, and W. Reichart, *Nucl. Phys.* **A257**, 317 (1976); P. G. Roos, N. S. Chant, A. A. Cowley, D. A. Goldberg, H. D. Holmgren, and R. Woody, III, *Phys. Rev. C* **15**, 69 (1977).
- ⁴⁰J. S. Wesick, Ph.D. thesis, University of Maryland, 1983.
- ⁴¹B. S. Podmore and H. S. Sherif, in *Few Body Problems in Nuclear and Particle Physics*, edited by R. J. Slobodrian, B. Cujec, and K. Ramavataram (Université Laval, Quebec, 1975), p. 517.
- ⁴²P. G. Roos (private communication).
- ⁴³A. A. Cowley, P. G. Roos, N. S. Chant, R. Woody, III., H. D. Holmgren, and D. A. Goldberg, *Phys. Rev. C* **15**, 1650 (1977).
- ⁴⁴T. K. Lim, *Phys. Lett.* **44B**, 341 (1973).
- ⁴⁵R. Schiavilla, V. R. Pandharipande, and R. B. Wiringa, *Nucl. Phys.* **A449**, 219 (1986).
- ⁴⁶J. M. Greben, *Phys. Lett.* **115B**, 363 (1982).
- ⁴⁷S. N. Bunker, J. M. Cameron, R. F. Carlson, J. Reginald Richardson, P. Tomaš, W. T. H. van Oers, and J. W. Verba,

- Nucl. Phys. **A113**, 461 (1968); E. A. Remler and R. A. Miller, Ann. Phys. (N.Y.) **82**, 189 (1974); H. Shimizu, K. Imai, N. Tamura, K. Nisimura, K. Hatanaka, T. Saito, Y. Koike, and Y. Taniguchi, Nucl. Phys. **A382**, 242 (1982); W. Gruebler, V. König, P. A. Schmelzbach, F. Sperisen, B. Jenny, R. E. White, F. Seiler, and H. W. Roser, *ibid.* **A398**, 445 (1983).
- ⁴⁸J. L. Detch, Jr., R. L. Hutson, Nelson Jarmie, and J. H. Jett, Phys. Rev. C **4**, 52 (1971); R. Darves-Blanc, Nguyen Van Sen, J. Arvieux, J. C. Gondrand, A. Fiore, and G. Perrin, Nucl. Phys. **A191**, 353 (1972); R. Darves-Blanc, Nguyen Van Sen, J. Arvieux, A. Fiore, J. C. Gondrand, and G. Perrin, Lett. Nuovo Cimento **4**, 16 (1972).
- ⁴⁹H. Langevin-Joliot, Ph. Narboni, J. P. Didelez, G. Duhamel, L. Marcus, and M. Roy-Stephan, Nucl. Phys. **A158**, 309 (1970).
- ⁵⁰S. A. Harbison, R. J. Griffiths, N. M. Stewart, A. R. Johnston, and G. T. A. Squier, Nucl. Phys. **A150**, 570 (1970); N. P. Goldstein, A. Held, and D. G. Stairs, Can. J. Phys. **48**, 2629 (1970); R. L. Hutson, Nelson Jarmie, J. L. Detch, Jr., and J. H. Jett, Phys. Rev. C **4**, 17 (1971); L. G. Votta, P. G. Roos, N. S. Chant, and R. Woody, III, *ibid.* **10**, 520 (1974); J. R. Morales, T. A. Cahill, D. J. Shadoan, and H. Willmes, *ibid.* **11**, 1905 (1975).
- ⁵¹Yoshiteru Kudo and Kiro Miyazaki, Phys. Rev. C **34**, 1192 (1986); Yoshiteru Kudo, Noriyo Kanayama, and Takashi Wakasugi, *ibid.* **38**, 1126 (1988); **39**, 1162 (1989).
- ⁵²Ranjan K. Bhowmik, C. C. Chang, J. P. Didelez, and H. D. Holmgren, Phys. Rev. C **13**, 2105 (1976).
- ⁵³Kenneth M. Watson, Phys. Rev. **88**, 1163 (1952); A. B. Migdal, Zh. Eksp. Teor. Fiz. **28**, 3 (1955) [Sov. Phys.—JETP **1**, 2 (1955)].
- ⁵⁴E. Lomon and Richard Wilson, Phys. Rev. C **9**, 1329 (1974).
- ⁵⁵M. Bernas, D. Bachelier, J. K. Lee, P. Radvanyi, M. Roy-Stéphan, I. Brissaud, and C. Détraz, Nucl. Phys. **A156**, 289 (1970).
- ⁵⁶F. R. Kroll and N. S. Wall, Phys. Rev. C **1**, 138 (1970).
- ⁵⁷C. Samanta, N. S. Chant, P. G. Roos, A. Nadasen, J. Wesick, and A. A. Cowley, Phys. Rev. C **34**, 1610 (1986).
- ⁵⁸A. A. Cowley, J. V. Pilcher, J. J. Lawrie, and D. M. Whittal, Phys. Rev. C **40**, 1950 (1989).
- ⁵⁹K. L. Lim and I. E. McCarthy, Nucl. Phys. **88**, 433 (1966); P. G. Roos, Phys. Rev. C **9**, 2437 (1974); Stephen K. Young and Edward F. Redish, *ibid.* **10**, 498 (1974); C. A. Miller, Nucl. Phys. **A353**, 157c (1981).
- ⁶⁰P. Kitching, W. J. McDonald, Th. A. J. Maris, and C. A. Z. Vasconcellos, in *Advances in Nuclear Physics*, edited by J. W. Negele and Erich Vogt (Plenum, New York, 1985), Vol. 15, p. 43.
- ⁶¹D. W. Devins, D. L. Friesel, W. P. Jones, A. C. Attard, I. D. Svalbe, V. C. Officer, R. S. Henderson, B. M. Spicer, and G. G. Shute, Aust. J. Phys. **32**, 323 (1979).
- ⁶²H. Tyrén, S. Kullander, O. Sundberg, R. Ramachandran, P. Isacson, and T. Berggren, Nucl. Phys. **79**, 321 (1966); C. F. Perdrisat, L. W. Swenson, P. C. Gugelot, E. T. Boschitz, W. K. Roberts, J. S. Vincent, and J. R. Priest, Phys. Rev. **187**, 1201 (1969).
- ⁶³Taber de Forest, Jr., Nucl. Phys. **A132**, 305 (1969); T. W. Donnelly, *ibid.* **A150**, 393 (1970); Y. Horikawa, F. Lenz, and Nimai C. Mukhopadhyay, Phys. Rev. C **22**, 1680 (1980).
- ⁶⁴D. M. Whittal, Ph.D. thesis, University of Cape Town, 1989.
- ⁶⁵G. Ciangaru, Phys. Rev. C **30**, 479 (1984).
- ⁶⁶D. F. Geesaman *et al.*, Phys. Rev. Lett. **63**, 734 (1989).
- ⁶⁷R. D. Smith and M. Bozoian, Phys. Rev. C **39**, 1751 (1989).
- ⁶⁸J. R. Wu, Phys. Lett. **91B**, 169 (1980).